LAPPEENRANTA UNIVERSITY OF TECHNOLOGY

LUT School of Engineering Science

Master's Degree Program in Chemical and Process Engineering

Rahul Prasad Bangalore Ashok

Hydrometallurgical process modeling using advanced mathematical tools

Examiners: Professor Tuomas Koiranen

                      Docent Arto Laari

Supervisor: M.Sc. (Tech) Vladimir Zhukov

ABSTRACT

Lappeenranta University of Technology

LUT School of Engineering Science

Master's Degree Program in Chemical and Process Engineering

Rahul Prasad Bangalore Ashok

Hydrometallurgical process modeling using advanced mathematical tools

Master's Thesis

2016

118 pages, 18 figures, 24 tables and 4 appendices

Examiners: Professor Tuomas Koiranen

                       Docent Arto Laari

Keywords: High pressure pyrite oxidation, zinc concentrate leaching, gold chloride leaching, reactor modeling, parameter estimation

Hydrometallurgical process modeling is the main objective of this Master's thesis work. Three different leaching processes namely, high pressure pyrite oxidation, direct oxidation zinc concentrate (sphalerite) leaching and gold chloride leaching using rotating disc electrode (RDE) are modeled and simulated using gPROMS process simulation program in order to evaluate its model building capabilities.

The leaching mechanism in each case is described in terms of a shrinking core model. The mathematical modeling carried out included process model development based on available literature, estimation of reaction kinetic parameters and assessment of the model reliability by checking the goodness fit and checking the cross correlation between the estimated parameters through the use of correlation matrices. The estimated parameter values in each case were compared with those obtained using the Modest simulation program.

Further, based on the estimated reaction kinetic parameters, reactor simulation and modeling for direct oxidation zinc concentrate (sphalerite) leaching is carried out in Aspen Plus V8.6. The zinc leaching autoclave is based on Cominco reactor configuration and is modeled as a series of continuous stirred reactors (CSTRs). The sphalerite conversion is calculated and a sensitivity analysis is carried out so to determine the optimum reactor operation temperature and optimum oxygen mass flow rate. In this way, the implementation of reaction kinetic models into the process flowsheet simulation environment has been demonstrated.

ACKNOWLEDGEMENTS

Table of Contents

List of Figures

List of Tables

List of Symbols

a	tolerance for absolute error, -
a_i	inner particle surface area, m^2
a_o	outer particle surface area, m^2
A_r	reaction surface area, m^2
A_i	particle reactive surface area, m^2
b	parameter used in experiment, $m^3\ mol^{-1}$
c	oxidant concentration in bulk liquid, $mol\ m^{-3}$
$c_{FeS_2,0}$	initial pyrite concentration, $mol\ m^{-3}$
$c_{Fe^{2+}}$	ferrous iron concentration, $mol\ m^{-3}$
$c_{Fe^{2+},mean}$	mean ferrous iron concentration, $mol\ m^{-3}$
$c_{Fe^{3+}}$	concentration of ferric ions, $mol\ m^{-3}$
$c_{Fe^{3+},mean}$	mean concentration of ferric ions, $mol\ m^{-3}$
c_{H^+}	hydrogen ion (H^+) concentration in liquid, $mol\ m^{-3}$
$c_{H_2SO_4}$	sulfuric acid concentration in liquid, $mol\ m^{-3}$
c_i	concentration at the inner particle surface, $mol\ m^{-3}$
$c_{O_2}^*$	dissolved oxygen concentration at saturation point, $mol\ m^{-3}$
c_{O_2}	dissolved oxygen concentration, $mol\ m^{-3}$
$c_{O_2,mean}$	mean dissolved oxygen concentration, $mol\ m^{-3}$
c_o	concentration at the outer particle surface, $mol\ m^{-3}$
$c_{O_2,s}$	concentration of dissolved oxygen at the reaction surface, $mol\ m^{-3}$
c_s	oxidant concentration at the disc surface, $mol\ m^{-3}$
c_{Zn}	zinc concentration in solids, $mol\ m^{-3}$
$c_{Zn,s}$	concentration of zinc at the surface in solids, $mol\ m^{-3}$
d	diameter of rotating disc, m
D	coefficient of diffusion, $m^2\ s^{-1}$
D^0	infinite dilution diffusion coefficient, $m^2\ s^{-1}$
D_e	effective particle diffusivity, $m^2\ min^{-1}$

d_i	inner particle diameter, m
d_0	outer particle diameter, m
E	activation energy, kJ mol^{-1}
E_1	activation energy, kJ mol^{-1}
E_2	activation energy, kJ mol^{-1}
E_3	activation energy, kJ mol^{-1}
E_4	activation energy, kJ mol^{-1}
E_5	activation energy, kJ mol^{-1}
E_6	activation energy, kJ mol^{-1}
F	Faraday constant, 96500 C mol^{-1}
F_{A_0}	inlet sphalerite mass flow, kg/h
F_A	outlet sphalerite mass flow, kg/h
k	reaction rate constant, -
K_{eq}	equilibrium rate constant, -
$k_{Fe^{2+}}$	rate constant for ferrous oxidation, -
$k_{Fe^{3+}}$	rate constant for ferric reduction, -
k_i	reaction rate constant, -
k_L	mass transfer coefficient across the boundary layer, mol m^2 s^{-1}
k_{mean}	reaction rate constant, mol m^{-2} s^{-1}
k_{O_2}	mass transfer coefficient of oxygen, s^{-1}
k_1	rate constant for pyrite oxidation, -
$k_{1,mean}$	rate constant for pyrite oxidation at mean temperature, mol m^{-2} s^{-1}
k_2	rate constant for ferric iron oxidation, -
$k_{2,mean}$	rate constant for ferric iron oxidation at mean temperature, mol m^{-2} s^{-1}
k_3	reaction rate constant for ferrous iron oxidation, -
$k_{3,mean}$	rate constant for ferrous iron oxidation at mean temperature, mol m^{-3} s^{-1}
k_4	reaction rate constant, -
$k_{4,mean}$	rate constant for ferrous iron oxidation at mean temperature, mol m^{-3} s^{-1}
k_5	reaction rate constant, -
$k_{5,mean}$	rate constant for ferrous iron oxidation at mean temperature, mol m^{-3} s^{-1}

k_6	reaction rate constant, -
$m_{f,Fe}$	mass fraction of Fe in ore, kg/kg
$m_{f,Zn}$	mass fraction of Zn in ore, kg/kg
n_1	parameter describing pyrite passivation, -
n_2	reaction order for dissolved oxygen, -
n_3	ferric ions reaction order, -
n_4	ferrous ions reaction order, -
n_5	dissolved oxygen reaction order (reaction R3), -
n_6	oxygen reaction order, -
n_7	sulfuric acid reaction order, -
n_8	reaction order for ferric iron (Fe^{3+}), -
n_9	sulphuric acid reaction order, -
n	number of particles per volume of reactor in the reactor, m^{-3}
n_d	number of differential variables involved in the problem, -
N	rotation speed of electrode, min^{-1}
N_E	total number of experiments performed, -
N_M	total number of measurements taken from all the experiments, -
$N_{M_{ij}}$	number of measurements of the jth variable in the ith experiment, -
N_{V_i}	number of measured variables in the ith experiment, -
P_{O_2}	oxygen partial pressure, kPa
p_{O_2}	partial pressure of oxygen, kPa
R	gas constant, 0.008314 kJ mol^{-1} K^{-1}
r	mass transfer rate of oxidant across the boundary layer, mol m^{-2} s^{-1}
r_e	tolerance for relative error, -
r_i	reaction surface radius, m
r_o	outer particle surface radius, m
r_s	reaction rate at the surface, mol m^2 s^{-1}
r_1	surface reaction rate between pyrite and oxygen, mol m^{-2} min^{-1}
r_2	surface reaction rate between pyrite and ferric ions, mol m^{-2} min^{-1}

r_3	reaction rate for reaction between ferrous iron and oxygen, mol m^{-3} s^{-1}
r_{-3}	backward reaction (ferric iron to ferrous iron) rate, mol m^{-3} s^{-1}
r_4	reaction rate at the surface for zinc oxidation by oxygen, mol m^{-2} min^{-1}
r_5	reaction rate at the surface for zinc oxidation by ferric iron (Fe^{3+}), mol m^{-2} min^{-1}
r_6	reaction rate at the surface for zinc oxidation by ferrous iron (Fe^{2+}), mol m^{-2} min^{-1}
T	temperature, K
T_{mean}	mean temperature, K
X_{FeS_2}	conversion of pyrite, %
$X_{FeS_2,mean}$	mean pyrite conversion, %
x_i	present value of the ith differential variable, -
y_i	experimental data values
$\tilde{z}_{ijk}$	kth measured value for variable j in experiment i, -
Z_{ijk}	kth predicted value for variable j in experiment i, -
Re	Reynolds number, $\frac{Nd^2}{v}$
Sh	Sherwood number, $\frac{k_L}{D}$
Sc	Schmidt number, $\frac{v}{D}$

Greek symbols

θ	set of model parameters that need to be estimated, -
σ_{ijk}^2	variance of the kth measurement for variable j in experiment i, -
ψ	shape factor, -
ε	liquid fraction volume in the slurry, m^3 m^{-3} slurry
μ^0	dynamic viscosity, kg m^{-1} s^{-1}
ϵ_i	local error estimate of the solver for the ith differential variable, -
v	kinematic viscosity, m^2 s^{-1}

1 Introduction

1.1 General background

The term hydrometallurgy can be defined as the branch of metallurgy that involves the study of the kinetics and the mechanism of extraction of metals from their ore concentrates by carrying out leaching in aqueous media. In Comparison with pyro-metallurgy, hydrometallurgy is still a still a recent technology with ongoing research and development (Van Weert, 1989).

There are three steps involved in hydrometallurgical processes for the extraction of metals from their ores or concentrates (Derry, 1972). In the first step, there is dissolution of the metal obtained from its ore or concentrate into a leaching solution. The second step involves further purification of the solution that is to be leached. Then finally the metal is recovered from the purified leach solution. Apart from these steps, there might often be pre-treatment stages involved such as pressure oxidation in case of refractory gold ores.

Hydrometallurgical leaching processes are limited by two factors namely, the rate at which the reaction proceeds (reaction kinetics) and the extent to which the leaching reaction proceeds. The total driving force for the reaction is dependent on the thermodynamic properties of the leaching system while the reaction kinetics takes into consideration the physico-chemical properties and mass transfer factors influencing the system.

1.2 Modeling

Mathematical modeling can be employed as a tool to study the leaching kinetics of the system. Several software programs are available commercially for the purpose of modeling and simulation. gPROMS (Process Systems Enterprise, 1997) is one such sophisticated modeling and simulation tool that is used in this thesis for modeling and simulating there different hydrometallurgical processes namely, high pressure pyrite oxidation, direct oxidative zinc

leaching and gold chloride leaching using rotating disc electrode. For each of these cases, the mathematical model can be formulated by taking into account the reaction kinetics, mass transfer phenomena and other process influencing factors like pressure, temperature, partial pressure of oxygen and mean particle size.

1.3 Objectives

The main objective of the Master's thesis work is the evaluation of the model builder feature in gPROMS by carrying out mathematical modeling for three different hydrometallurgical leaching processes, estimation of the unknown model parameters and study of the model reliability, comparison of the results obtained in gPROMS with those obtained from the Modest software program. Reactor modeling in Aspen plus (v. 8.6) for direct oxidative zinc leaching case in a series of continuous stirred reactors by using the estimated reaction kinetic parameters was an additional objective. The main aim of reactor modelling was to introduce the benefits of modeling into process flowsheet simulation from a process design perspective.

2 Hydrometallurgical leaching processes

One of the most important processes involved in hydrometallurgy is leaching. During the leaching process, the ore or the concentrate is treated with a chemically active solution called the leach solution so as to facilitate the dissolution of the minerals selectively. Normally acids are employed as the leaching agents because of their capability to leach both base and precious metals.

As part of the this Master's thesis, three different hydrometallurgical processes namely high pressure oxidation, direct oxidative zinc leaching and gold chloride leaching using rotating disc electrode have been discussed in detail.

The pressure oxidation process is considered to be one of the main techniques for the leaching of gold from its ore. Pressure oxidation involves complete or partial oxidation of the refractory minerals present in the ore concentrate, thereby subjecting gold to leaching in the presence of acidic conditions.

Hydrometallurgical treatment process like direct oxidative leaching is normally used to extract zinc from its ore concentrate. This is done in the presence of an acidic media like suphuric acid. The direct oxidation leaching kinetics is rather complex and involves multi-phase mass transfer, reactive area shrinkage and internal particle diffusion.

The gold chloride leaching using rotating disc electrode (RDE) is based on the gold dissolution model, in which the mass transfer occurring on the disc surface is expressed in terms of dimensionless numbers like Reynolds number, Schmidt number and Sherwood number. The RDE studies give information about the main mechanisms involved during leaching of gold in chloride solutions.

2.1 Gold leaching using high pressure pyrite oxidation process

2.1.1 Process overview

It has been observed that in case of sulfide containing ores such as pyrite, arsenopyrite and chalcopyrite, gold is present in the form of minute particles that are embedded within the sulfide structure of the ores. So as to improve and enhance the recovery of gold particles from these sulfidic ores, one of the most commonly employed method is high pressure pyrite oxidation process (Zhukov et al, 2015).

Generally, the pressure oxidation process is carried out in high pressure reactors which act as complex three phase systems and which include precipitation and dissolution reactions that depend upon the process chemistry, conditions of temperature and pressure existing within the reactor (Baldwin, et al., 1998). The leaching mechanism in pressure oxidation is dependent on the kinetics of the reaction and species mass transfer rate.

The interactions between components in a 3-phase system can be described by making use of a shrinking core kinetic model (SCM). As per the SCM model, the initial reaction starts at the outer surface of the reacting particle and as the reaction proceeds, converted material and unreacted solid commonly referred to as "ash" (Levenspiel, 1999) is left behind. Therefore, at any particular instant, there always exists an unreacted material core which continuously undergoes shrinkage as the reaction proceeds as shown in Figure 1.

To completely understand the reaction mechanism involved during pressure oxidation process, we also need to include the oxygen mass transfer into the surrounding bulk liquid and into the solid particles that are oxidized subsequently. Therefore, there are 4 main steps involved in pressure oxidation as shown below:

- Step 1: Mass transfer of oxygen into the solution phase (Fig. 1, position 1 and 2).

- Step 2: Mass transfer of dissolved oxygen across the boundary layer into the solid mineral surface. (Fig. 1, position 3).

- Step 3: Electrochemical reaction at the surface of the solid (Fig. 1, position 4-7). which usually includes the following sub stages:

  - Hydroxylation-hydration at the surface
  - Surface species reaction
  - Reacting species adsorption on the surface of the solid.
  - Product species desorption from the surface of the solid
  - Product reaction within the solution

- Step 4: Mass transfer of the product species across the boundary layer into the bulk solution (Fig. 1, position 8).
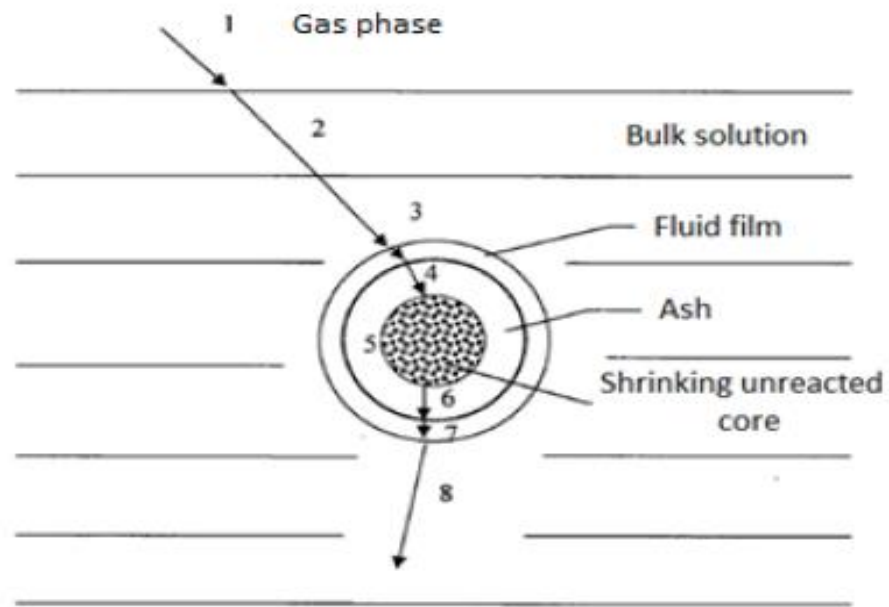
Figure 1. Shrinking core model schematic representation (Levenspiel, 1999)

The block diagram representation of the pressure oxidation process is shown in Figure 2:

18
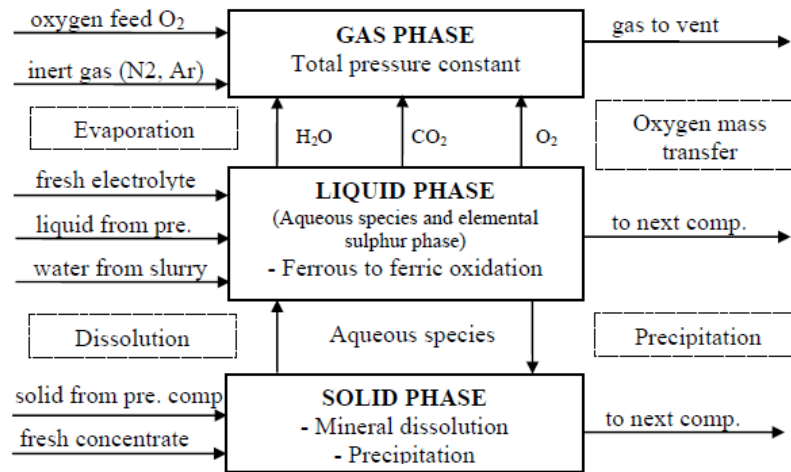
Figure 2. Block diagram for the pressure oxidation process (Baldwin, et al., 1998).

2.1.2 Process chemistry

High pressure pyrite oxidation is carried out in sulfuric acid solution at high temperatures (usually above 170^0C). Over the years, the pyrite oxidation process has been studied extensively. In one such research, Long and Dixon carried out the high pressure pyrite oxidation on a laboratory scale in acidic conditions. They found that the pyrite oxidation process was dependent on pyrite conversion, partial pressure of oxygen and particle diameter (Long and Dixon, 2004).

The pyrite oxidation process is very much complicated as it includes many surface and bulk phase reactions. In fact, over the years, there has been ongoing debate about the different kinds of reaction mechanisms involved during the process. However, there has been a general consensus that the reaction proceeds according to an electrochemical mechanism.

Usually at high temperatures and in the presence of acidic medium (H_2SO_4), the pyrite reacts with dissolved oxygen and ferric ion (Fe^{3+}) as shown by the following two reactions which occur at the surface of the pyrite (Bailey and Peters, 1976):

19

$$FeS_2 + 3.5O_2 + H_2O \rightarrow Fe^{2+} + 2SO_4^{2-} + 2H^+ \tag{R1}$$

$$FeS_2 + 14Fe^{3+} + 8H_2O \rightarrow 15Fe^{2+} + 2SO_4^{2-} + 16H^+ \tag{R2}$$
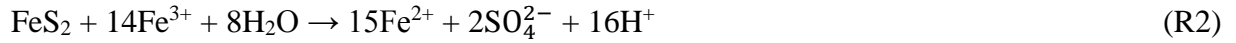
As the reaction proceeds, the ferrous ion (Fe^{2+}) produced in reaction R1 undergoes oxidation to ferric ion (Fe^{3+}) as shown below by the bulk phase liquid reaction R3:

$$Fe^{2+} + 0.25O_2 + H^+ \rightarrow Fe^{3+} + 0.5H_2O \tag{R3}$$

It was shown by Moses et al. (1987) that at ambient conditions, the reaction R2 with Fe^{3+} as the oxidant proceeds relatively faster in comparison to the reaction R1 with molecular oxygen as the oxidant. Therefore, the reaction R1 is taken into consideration only when the dissolved iron concentration is low. In some cases, when the reaction R2 is considerably fast, reaction R3 controls the overall rate of leaching and acts as a limiting factor.

Long and Dixon found based on their pressure oxidation experimental study that at low slurry concentrations there is passivation on the surface. It is caused due to the presence of elemental sulphur. They came to a conclusion that instead of reaction R1, the oxidation reaction instead results in the production of thiosulphate which subsequently breakdown to form elemental sulphur as shown in reactions R4 and R5, respectively.

$$FeS_2 + 1.75O_2 + H^+ \rightarrow Fe^{3+} + S_2O_3^{2-} + 0.5H_2O \tag{R4}$$

$$S_2O_3^{2-} \rightarrow S + SO_3^{2-} \tag{R5}$$
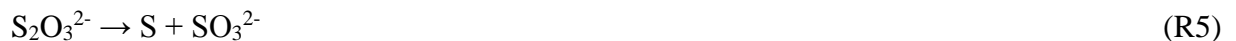
Furthermore, the resulting thiosulphate undergoes oxidation in presence of ferric ion to form sulfate as shown in reaction R6.

$$S_2O_3^{2-} + 2Fe^{3+} + H_2O \rightarrow SO_4^{2-} + 2Fe^{2+} + 2H^+ \tag{R6}$$

The kinetics involved in pyrite oxidation have already been investigated in many studies. According to Holmes and Crundwell (2000), during pyrite dissolution, an electrochemical mechanism is involved in which the rate is controlled by charge transfer at the surface and solution interface. Based on this mechanism, a rate equation for the pyrite dissolution by ferric ions and dissolved oxygen was derived as shown in Equation (1).

$$r_{FeS_2} = \frac{k_{FeS_2} c_{H^+}^{-1/2}}{14F} \left(\frac{k_{Fe^{3+}} c_{Fe^{3+}} + k_{O_2} c_{O_2} c_{H^+}^{0.14}}{k_{FeS_2} c_{H^+}^{-1/2} + k_{Fe^{2+}} c_{Fe^{2+}}} \right)^{0.5} \tag{1}$$

Where,

r_{FeS_2} pyrite oxidation reaction rate, mol m^{-3} s^{-1}

k_{FeS_2} pyrite oxidation reaction rate constant, -

c_{H^+} hydrogen concentration, mol m^{-3}

F Faraday constant, 96500 C mol^{-1}

$k_{Fe^{2+}}$ rate constant for ferrous oxidation, -

$k_{Fe^{3+}}$ rate constant for ferric reduction, -

k_{O_2} mass transfer coefficient of oxygen, s^{-1}

$c_{Fe^{3+}}$ concentration of ferric ions, mol m^{-3}

c_{O_2} concentration of dissolved oxygen, mol m^{-3}

As per Equation 1, the reaction order is about 0.5 with respect to the dissolved oxygen in low concentration of iron. When the ion concentration is high, anions like Cl^- and SO_4^{2-} have an inhibiting effect on the rate of pyrite oxidation. This is due to the adsorption of anions on the surface of the pyrite which inhibit the oxidizing capability and thereby have a detrimental effect on the rate.

The rate of ferrous ion oxidation is of first order with respect to the concentration of ferrous ion and oxygen (Garrels and Thompson (1960) and Singer and Stumm (1970)),

$$-\frac{dc_{Fe^{2+}}}{dt} = kc_{Fe^{2+}}c_{O_2} \qquad\qquad (2)$$

Where,

$c_{Fe^{2+}}$ ferrous iron concentration, mol m^{-3}

c_{O_2} dissolved oxygen concentration at saturation point, mol m^{-3}

Based on the mechanisms described above, it can be easily seen that the pyrite oxidation process is complicated and it includes reactions that occur on the surface and in the bulk phase. The leaching rate is found to depend on factors such as temperature, oxygen partial pressure, average size of particles and concentration of the reactants.

2.2 Zinc concentrate leaching

2.2.1 Process overview

Zinc normally exists in the form of sulfides and the most important ore being sphalerite (ZnS). The main raw material for zinc extraction is zinc sulfide concentrate. In most researches, hydrometallurgical processes have been adopted for producing zinc from its ore concentrate. The processes reported include roasting process in which toxic sulphur dioxide (SO_2) is released into the atmosphere.

Hydrometallurgical processes such as direct oxidation leaching that do not involve any pre-treatment steps are being considered as the popular choices for the extraction of zinc from its concentrate ore. On a commercial scale, the process of pressure leaching has been applied to metal ores and concentrates as it offers advantages such as better control, optimum mineral utilization and improved flexibility. The leaching of zinc concentrates by direct oxidation in the presence of acidic conditions is a complicated process. It includes reaction between several components at the concentrate reactive surface, shrinkage in the reactive area as the reaction proceeds, internal diffusion within the particles and multi-phase mass transfer reactions which limit access of reactants to the reactive surface area.

Direct oxidative leaching can be divided into two types, namely atmospheric leaching in which the leaching is carried out under atmospheric pressure and pressure leaching in which the leaching proceeds at elevated pressure conditions (Haakana et al. 2007).

In atmospheric leaching, the leaching is carried out at atmospheric pressure and the temperature is maintained at 100 ^{0}C (Filippou 2004). Slight changes in the reaction conditions can produce different reaction rates. In comparison to pressure leaching, atmospheric leaching reaction proceeds at a slower rate and therefore has a much higher retention and residence time (Takala, 1999). So far, many commercial atmospheric leaching processes have been developed as such as Union Miniere Direct leach process, Outokumpu Concentrate leach process and the MIM Albion Concentrate leach process (Filippou, 2004).

Pressure leaching is normally used for low grade zinc concentrate ores consisting of impurities like copper, lead, iron etc. Using pressure leach technology, almost all the sulphidic raw materials can be reprocessed (Kazanbaev et al., 2007). Pressure leaching can be further divided into low temperature and high temperature pressure leaching from the industrial application viewpoint.

Low temperature pressure leaching was first introduced on pilot scale basis by Cominco in Trail during 1962-1963 (Sequeira and Marquis, 1997). The leaching was carried out in an autoclave reactor that consisted of four chambers. The reaction temperature was maintained at 110 ^{0}C while the oxygen pressure was varied between 0.7 bar - 4.2 bar. The residence time within the reactor was six hours and the final leaching yield of zinc was around 96 percent (Sequeira and Marquis, 1997).

However, low temperature pressure leaching is yet to be introduced on an industrial scale due to problems associated with high residence times and difficulties in controlling the temperature. The conditions employed during low temperature pressure leaching is shown below in Table 1.

Table 1. Low temperature pressure leaching conditions (Kazanbaev et al., 2007)

Process conditions	Value
Temperature, ^{0}C	107
Oxygen partial pressure, bar	2 - 3
Residence time, h	3 - 4
Number of stages	1
Zinc leaching yield, %	96 -97

High temperature pressure leaching is carried out at temperatures above the melting point of sulphur (147 – 152 ^{0}C). Sulphur films may be formed on the sphalerite surface in case any melted sulphur is present in the leaching solution. To avoid this, sulphur active agents are usually incorporated into the leaching solution. The residence time of the process is 2 hours and the leaching yield of zinc is around 98 percent. (Sequeira and Marquis, 1997).

Table 2. High temperature pressure leaching conditions (Kazanbaev et al., 2007)

Process conditions	Cominco (Trail, Canada)	Kiddcreek (Trimmins, Canada)	Ruhr-Zink (Datteln, Germany)	Hudson Bay (Flin Flon, Canada)
Plant capacity, t/d	190	100	290	520
Temperature, ^{0}C	147 - 157	147 – 177	150	145 - 150
Partial pressure of oxygen, bar	12	17	16	-
Residence time, h	1.4	2	1.5	2 stages
Zinc leaching yield , %	97	98	98	99

High temperature pressure leaching is found to be more efficient in comparison to low temperature pressure leaching and this can be attributed to the following reasons (Kazanbaev et al., 2007):

- Increased zinc leaching yield by 2 to 5 percent.
- Decreased process residence time by 2 – 3 times.
- Decreased consumption of sulphuric acid by 10 – 20 percent.

2.2.2 Process chemistry

The kinetics involved in leaching of zinc sulfide concentrates have already been studied in great detail and most authors have suggested the use of shrinking core model in order to describe the process. Souza et al. (2007) in their study investigated the leaching of zinc concentrates in the presence of acidic ferric sulphate solution and the effect of temperature, concentrations of ferric ion and sulfuric acid, stirring speed and average particle size on the process. The kinetic parameters involved in the process were obtained by applying the shrinking core model.

Xie et al. (2007) in their study also utilized a similar approach to investigate the kinetics involved in zinc concentrate pressure leaching. The kinetics of leaching in acidic ferric chloride solution was studied by Aydogan et al. (2005). Based on their study, it was concluded that the leaching process is limited by reaction rate and an empirical correlation was introduced in order to represent the rate of dissolution of zinc.

The leaching reaction is carried out in the presence of acidic medium such as sulphuric acid and oxygen (Filippou, 2004). The overall reaction taking place during direct oxidative zinc leaching has been shown below (Maslenetsky et al., 1969):

$$ZnS + H_2SO_4 + 0.5O_2 \rightarrow MeSO_4 + S^0 + H_2O \tag{R7}$$

The above reaction proceeds slowly in case the concentration of the iron in the solution is very low. The iron concentration in the solution is responsible for the oxygen transfer and hence affects the rate of the reaction (Kaskiala, 2005 b). Kammel et al. (1987) in their study observed that the rate of zinc leaching improved gradually with addition of ferric iron sulphate in small amounts.

The metal sulfides present in the zinc concentrate are oxidized by the ferric ions according to the reaction shown below (Takala, 1999):

$$Fe_2(SO_4)_3 + MeS \rightarrow 2FeSO_4 + MeSO_4 + S^0 \tag{R8}$$
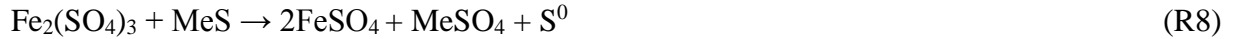
Where,

Me is the metal under consideration (Zn, Fe, Cu, etc.)

Successful sphalerite leaching experiments were carried out by Bjorling (1956) and Forward and Veltman (1959). Bjorling (1956) described the metal sulphide oxidation in the presence of aqueous sulphuric acid medium by making use of the following reaction R9.

$$MeS + H_2SO_4 + 0.5O_2 \rightarrow MeSO_4 + S + H_2O \tag{R9}$$

Where,

Me metal under consideration (Zn, Fe, Cu, etc.)

It was observed by Bjorling (1956) that the metal (Zinc) sulphide oxidation reaction proceeded very slowly and hence required the presence of a catalyst for making the reaction feasible.

Forward and Veltman (1959) in their study noted the role of iron as a catalyst present in concentrates in the form of marmatite and as other impurities. Later, Mackie and Veltman (1967) and Veltman et al. (1972) also reported the reaction mechanism for zinc oxidation in the presence of ferric iron as shown below.

$$ZnS + Fe_2(SO_4)_3 \rightarrow ZnSO_4 + 2FeSO_4 + S \tag{R10}$$

In the presence of oxygen, the ferrous iron undergoes oxidation to ferric iron according to the reaction R11.

$$2FeSO_4 + H_2SO_4 + 0.5O_2 \rightarrow Fe_2(SO_4)_3 + H_2O \tag{R11}$$

2.3 Gold chloride leaching using RDE

2.3.1 Process overview

Chlorination is often employed for the leaching of gold ore concentrates. Since the introduction of the cyanidation, the use of the chlorination process has declined gradually and nowadays is only used in the process of gold refining (Feather et al., 1997).

In the presence of aqueous chloride solutions and strong oxidizing agents, gold dissolves to give Au (I) and Au (III) chloride complexes. There are two steps involved during gold dissolution. In the first step, there is Au (I) chloride formation at the surface of gold and in the next step, $AuCl_2^-$ formation occurs. Based on the solution oxidizing potential, $AuCl_2^-$ may undergo further oxidation to form $AuCl_4^-$ (Filmer et al., 1984).

$$AuCl_2^- + e^- \rightarrow Au + 2Cl^- \tag{R12}$$

$$AuCl_4^- + 3e^- \rightarrow Au + 4Cl^- \tag{R13}$$

Since the reaction proceeds at a fast rate and in the presence of acidic conditions, there is no surface passivation problem.

2.3.2 Mass transfer in rotating disc electrode (RDE)

The mechanism of mass transfer onto the rotating disc surface has been reported by several authors (Sulaymon and Abbar, 2012; Dib and Makhloufi, 2007). Sulaymon and Abbar (2012) in their study investigated the mass transfer process taking place on to the surface of an amalgamated copper rotating disc electrode (RDE). They later concluded that in case of a rotating disc electrode, the mass transfer can be expressed in terms of dimensionless numbers like Sherwood number, Reynolds number and Schmidt number.

Dib and Makhloufi (2007) in their study reported the reaction kinetics and mass transfer mechanism taking place in nickel and cobalt cementation from zinc sulphate solution by making use of a rotating zinc electrode. Based on their study, it was again concluded that mass transfer could be easily expressed in terms of dimensionless numbers.

Thus, for comparing the different mass transfer mechanisms, dimensionless numbers (Sherwood, Reynolds and Schmidt number) can be used in place of mass transfer coefficient and the superficial velocity.

In case of a rotating disc electrode (RDE), the mass transfer can be expressed in terms of dimensionless numbers as follows.

$$Sh = a_1 Re^{a_2} Sc^{1/3} \qquad\qquad (3)$$

$$Sh = \frac{k_L}{D} \qquad\qquad (4)$$

$$Re = \frac{Nd^2}{v} \qquad\qquad (5)$$

$$Sc = \frac{v}{D} \qquad\qquad (6)$$

Where,

Sh Sherwood number, -

Re Reynolds number, -

Sc Schmidt number, -

d diameter of rotating disc, m

D coefficient of diffusion, $m^2 \, s^{-1}$

N electrode rotating speed, min^{-1}

v kinematic viscosity, $m^2 \, s^{-1}$

The effect of temperature on the diffusion coefficient and kinematic viscosity need to be taken into consideration for calculating the mass transfer rate. Li and Gregory (1974) in their study reported the diffusion coefficient values for Cu^{2+} and Fe^{3+} at 298.15K and infinite dilution as 7.33×10^{-9} m^2/s and 6.09×10^{-9} m^2/s respectively. Stokes-Einstein relation can be utilized for correction of temperatures.

$$\left(\frac{D^0 \mu^0}{T}\right)_{T_1} = \left(\frac{D^0 \mu^0}{T}\right)_{T_2} \tag{7}$$

Where,

D^0 infinite dilution diffusion coefficient, m^2 s^{-1}

μ^0 dynamic viscosity, kg m^{-1} s^{-1}

The effect of ionic concentration on the diffusion coefficient and on the viscosity are not taken into consideration. The effect is complicated and would require experimental verification at different ionic concentrations.

The estimated diffusion coefficient values for Cu^{2+} and Fe^{3+} at different temperatures based on the data obtained from Li and Gregory (1974) and Equation (42) are shown in Table 3.

Table 3. Dependence of water viscosity and diffusion coefficient on temperature (Li and Gregory, 1974)

T, K	μ , m Pa s	$D^0_{Cu^{2+}}$, m^2 s^{-1}	$D^0_{Fe^{3+}}$, m^2 s^{-1}
298.15	0.890	7.33E-9	6.07E-9
338.15	0.433	1.71E-8	1.42E-8
348.15	0.378	2.02E-8	1.67E-8
358.15	0.334	2.35E-8	1.94E-8
368.15	0.298	2.70E-8	2.24E-8

3 gPROMS as process modeling and parameter estimation tool

3.1 Introduction

gPROMS (Process Systems Enterprise, 1997) is a highly specialized general process modeling software that is used for carrying out predictive process system modelling and simulation by many leading process industries and research institutions all around the world.

It finds its main application in process engineering activities related to system modeling, equipment design and development and process operation optimization. In addition to this, transient systems that are described in terms of algebraic, partial derivative and integral equations can be modeled easily in gPROMS (gPROMS Introductory User Guide, 2004).

Some of the cases for which gPROMS can be adopted are as follows:

- Process simulation
- Parameter estimation
- Process optimization

3.2 Features of gPROMS

Compared to the traditional process modeling and simulation tools, gPROMS offers many features. It:

- Incorporates a multiscale modeling environment wherein it is possible to take all process conditions and phenomenon into consideration.

- Offers excellent process modeling ability that allows the user to create, develop and execute models with high fidelity for a wide range of equipment and then subsequent integration of these models into the process flowsheet.

- Incorporates the parameter estimation tool, which can be used for carrying out dynamic and steady state modeling wherein it is possible to estimate the parameters of a process model based on existing experimental data and industrial pilot scale studies.

- Has ability to execute multi-parameter models that involve complex process and detailed mathematical modeling using state of the art optimization numerical solvers capable of handling both lumped and distributed parameter systems.

- Has powerful optimization capabilities in comparison to the traditional trial and error simulations, thereby allowing the user to simulate steady state and dynamic process models.

- Includes Custom modeling capability to create user friendly models devoid of any complexity. gPROMS uses a natural mathematical language wherein the process model can be described accurately without the need for any extensive programming.

- Has solvers which are designed for use in case of large scale systems with no limitation in terms of problem size. As a result, it can be used to describe any process system in terms of mathematical modeling.
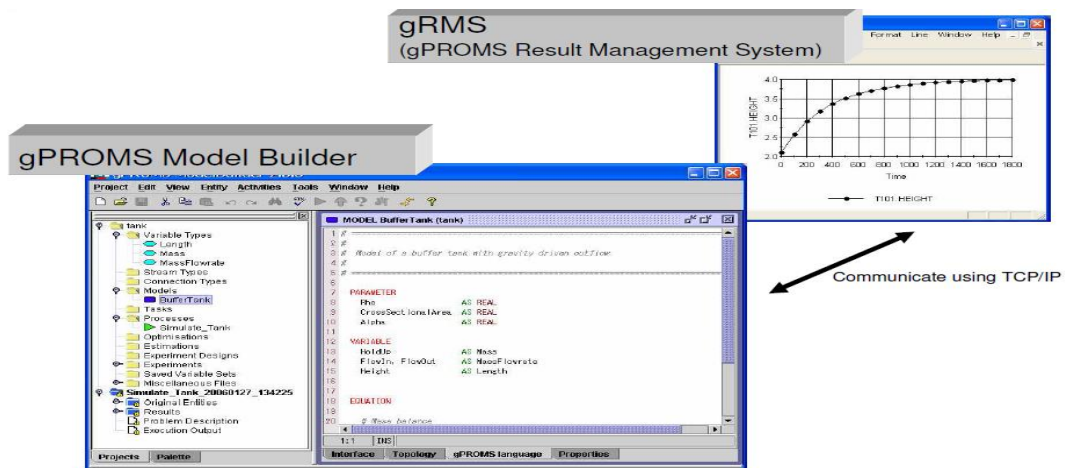
Figure 3. gPROMS basic interface

3.3 gPROMS solvers

gPROMS includes several categories of numerical solvers for carrying out process simulation, optimization and parameter estimation (gPROMS Introductory User Guide, 2004):

- Numerical solvers for linear equations
  gPROMS includes two important numerical solvers MA28 and MA48 for solving systems of linear equations. Both the solvers make use of the LU-factorization algorithm that is employed for solving large, sparse and asymmetric system of linear equations.

- Numerical solvers for non-linear algebraic equations
  There are three different types of numerical solvers available in gPROMS for solving systems of nonlinear equations:

  o BDNLSOL
    BDNLSOL is a general block decomposition solver for solving systems of non-linear equations. It makes use of a novel solving algorithm with a capability for handling equations with reversible symmetric discontinuities.

  o NLSOL
    NLSOL is a general non-linear solver, with and without block decomposition. It is implemented in gPROMS by providing access to the existing available non-linear solvers. Therefore, NLSOL cannot be considered as a true software component and is suited as a non-linear solver only for simulation purposes.

  o SPARSE
    SPARSE is a sophisticated solver used for implementing Newton type equations and does not include block decomposition.

- Numerical Solvers for mixed system of non-linear and differential equations

  gPROMS also includes two numerical solvers DASOLV and SRADAU for solving systems involving differential and algebraic equations. These solvers are even capable of handling partial derivative equations.

  - DASOLV

    The DASOLV solver makes use of the variable time step backward differentiation formulae (BDF). Solvers based on BDF are suited for solving systems that involve frequent discontinuities and high oscillatory behavior.

  - SRDAU

    The SRDAU solver makes use of fully implicit variable time step Runge-Kutta method. This solver is efficient for solving system of equations involving discretization and frequent discontinuities.

    In case of both the solvers (DASOLV and SRDAU), the time step is taken into consideration based on the following criterion:

    $$\sqrt{\frac{1}{n_d}\sum_{i=1}^{n_d}\left(\frac{\epsilon_i}{a+r_e|x_i|}\right)^2} \leq 1 \qquad (8)$$

    Where,

    n_d number of differential variables involved in the problem, -

    ϵ_i local error estimate of the solver for the ith differential variable, -

    x_i present value of the ith differential variable, -

    a tolerance for absolute error, -

    r_e tolerance for relative error, -

- Numerical solvers for optimization

  Two numerical solvers are available in gPROMS, namely CVP_SS and CVP_MS for solving optimization problems under steady state and dynamic conditions. The solvers for optimization are usually specified within the Solution Parameters section while defining the process entity.

  - CVP_SS

    CVP_SS solver is used for mixed integer optimization problems involving both discrete and continuous decision variables. It makes use single-shooting dynamic optimization algorithm.

  - CVP_MS

    CVP_MS solver is used for dynamic optimization problems involving continuous decision variables. It makes use of multiple shooting dynamic optimization algorithm.
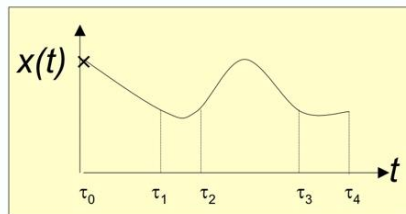
(a) Single-shooting algorithm   (b) Multiple-shooting algorithm
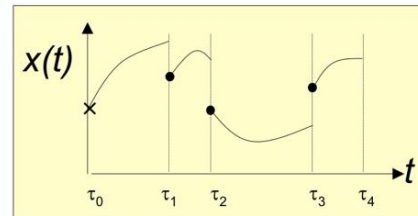
Figure 4. Single and multiple shooting algorithms

In case of dynamic optimization, both the solvers (CVP_SS and CVP_MS) make use of an approach based on parametrization in which it is assumed that the variables are piecewise constant functions of time over a determined interval range.

3.4 Parameter estimation in gPROMS

One of the important applications of gPROMS is its parameter estimation capability. On the basis of existing experimental results, it is possible to estimate the parameter values that affect the process. For the parameter estimation, it is possible to make use of either steady state or dynamic experiments that would usually involve different process initial conditions and operation sequences (gPROMS Advanced User Guide, 2004) .

Figure 5. Schematic for parameter estimation model development (Tjil, 2005)

3.5 Solving method

In general, for parameter estimation problems in gPROMS, the parameters are evaluated on the basis of an objective function that undergoes minimization. The objective function along with the numerical solver constitutes the solving method. Usually there is one objective function that is minimized by making use of a specific solver that is selected depending on the type of system (linear or non-linear) that would be handled. In Fig. 6, it can be clearly seen how the solving method is implemented in gPROMS.

Software package	gPROMS
Objective function	Max log likelihood
Optimisation solver	MXLKHD (indirect)
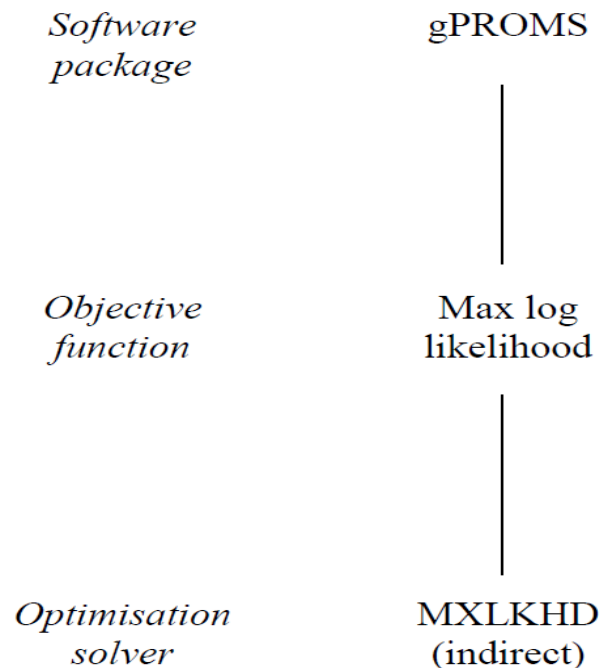
Figure 6. gPROMS solving methodology (Tjil, 2005)

As mentioned above, the parameter estimation in gPROMS involves determining the values of the unknown parameters so as to increase the probability of the mathematical model to estimate the parameter values accurately based on the experimental values. The objective function equation that is implemented on the basis of maximum likelihood approach in gPROMS has been presented below (gPROMS Introductory User Guide, 2004)

$$\phi = \frac{N_M}{2} \ln(2\pi) + \frac{1}{2} min_\theta \left\{ \sum_{i=1}^{N_E} \sum_{j=1}^{N_{Vi}} \sum_{k=1}^{N_{Mij}} \left[\ln(\sigma_{ijk}^2) + \frac{(\tilde{z}_{ijk} - z_{ijk})^2}{\sigma_{ijk}^2} \right] \right\} \tag{9}$$

Where,

N_M total number of experimental measurements, -

θ set of model parameters that need to be estimated, -

N_E total experiments carried out, -

N_{Vi} number of measured variables in the ith experiment, -

N_{Mij} number of measurements of the jth variable in the ith experiment, -

σ_{ijk}^2 variance of the kth measurement for variable j in experiment i, -

$\tilde{z}_{ijk}$ k^{th} measured value for variable j in experiment i, -

Z_{ijk} k^{th} predicted value for variable j in experiment i, -

3.6 Development of process model using gPROMS

3.6.1 Model builder

All processes are modeled in the gPROMS model builder environment. In the model builder, all the active projects can be seen under the project tree which includes the following sections.

- Variable declaration
- Model declaration
- Tasks specification
- Process implementation
- Experiment Design
- Process optimization
- Parameter estimation

3.6.2 Model definition

Models are used to describe the physical and chemical conditions of any process to be implemented in terms of mathematical modeling.

In general, a model in gPROMS incorporates the following sections:

- Parameter definition

  Parameters refer to constant values or parameters to be estimated by simulation. Within the parameter definition section, it is possible to declare three constant types (Real, Integer and Logical). The parameter values defined remain constant throughout the process simulation.

- Variable types definition

  Within the variable section, all the parameters that need to be estimated as a result of simulation are defined. Variables can be time dependent or time invariant. Usually, the variable values can be either assigned or estimated by simulation.

- Unit definition

  The process unit that needs to be utilized for carrying out the process modeling is defined in the unit section.

- Task Specification

  The external influences and actions to be imposed on the system under consideration are defined in the task specification section.

- Equations

  The differential and algebraic equations are defined under this section. Also by making use of the partial and integral operators, it is possible to define partial derivative

equations and integral functions. For handling equations that are conditional, deferent operators such as WHEN…END, CASE…END can be made use of.

3.6.3 Process definition

The process entity in gPROMS incorporates all the necessary information for defining a simulation. The various sections included within the process entity have been shown below:

- Unit specification

  Within this section, all the specific units that are to be incorporated in the modeling and simulation activity are indicated.

- Parameter values definition

  Within this section, values are assigned to all the parameters defined in the model file

- Variable values definition

  The model input values are specified in this section. Usually, in case of a process model, the number of variables used exceed the number of equations. Hence, so as to equate the number of variables to the number of equations and avoid under or over specification of the system, additional variables can be assigned in this section as well.

- Process initial conditions

  The initial process conditions for the simulation activity are defined in this section. gPROMS considers the initial conditions as general equations and as a result, the initial state value can be estimated in terms of an equation instead of assigning it as a constant value.

- Parameters solution specification

  The result parameters and the type of mathematical solver to be used for carrying out the simulation activity (optimization and parameter estimation) can be specified using solution parameters section.

- Process schedule definition

  Within this section, the process operation schedule is defined. One of the primary objectives in modeling is to investigate the behavior of model under different operating conditions. These conditions or manipulations can be described by the process schedule.

3.7 Comparison of gPROMS with existing process modeling software packages

Many popular software packages for carrying out process simulation, process optimization, process control and design like ASPEN (Aspen Technology Inc, 1981), Matlab (MathWorks Inc, 1984), MODEST (Harrio, 2002) and CHEMCAD (Chemstations Inc, 1988) are available commercially so as to describe the transient response of process operations by making use of differential partial derivative and algebraic equations (DAEs).

Tjil (2005) evaluated and compared the modelling capabilities of Aspen Custom Modeler (ACM) with that of gPROMS in order to carry out optimization for the Sec-Butanol stripping process. The stripping process was simulated and modeled using both Aspen Custom modeler and gPROMS and their modeling capabilities were evaluated by carrying out parameter estimation.

Using the two softwares (ACM and gPROMS), various parameter estimation aspects like input of experimental data, interpretation of output, solving strategies, objective function and solvers were evaluated. Tjil (2005) based on his study found that the solvers incorporated within gPROMS proved to be more powerful and showed better handling capability for obtaining optimum parameter estimates in comparison to Aspen Custom Modeler (ACM). In addition to this, the statistical information provided in gPROMS was found to be extensive leading to better model reliability and therefore it was concluded that the parameter estimation capabilities in gPROMS proved to be better in comparison to Aspen Custom Modeler (ACM).

As a part of the thesis, the parameter estimation capability of gPROMS will be evaluated and compared with that of the Modest program. A comparison between these two software packages on the basis of performance and handling capability has been shown in Table 4.

Table 4. Comparison of gPROMS with Modest

Feature	gPROMS	Modest
About	Specialized general process modeling software package for predictive system modeling and simulation.	Software package designed for mathematical modeling, parameter estimation and experimental design.
Coding language	Does not require the use of any programming language.	Requires the use of coding language Fortran 77.
Handling capability	Supports several categories of solvers for solving systems of linear, non-linear, differential and partial derivative equations.	Capability to handle linear and non-linear systems of algebraic equations and differential equations
Objective function	Objective function is based on maximum likelihood approach	Objective function is based on sum of residual squares
Main applicability	Main applications in: • Process simulation • Parameter estimation • Process optimization • Experimental design	Main applications in: • Parameter estimation • Design of experiments • Sensitivity analysis • Process optimization

4 Applied Part
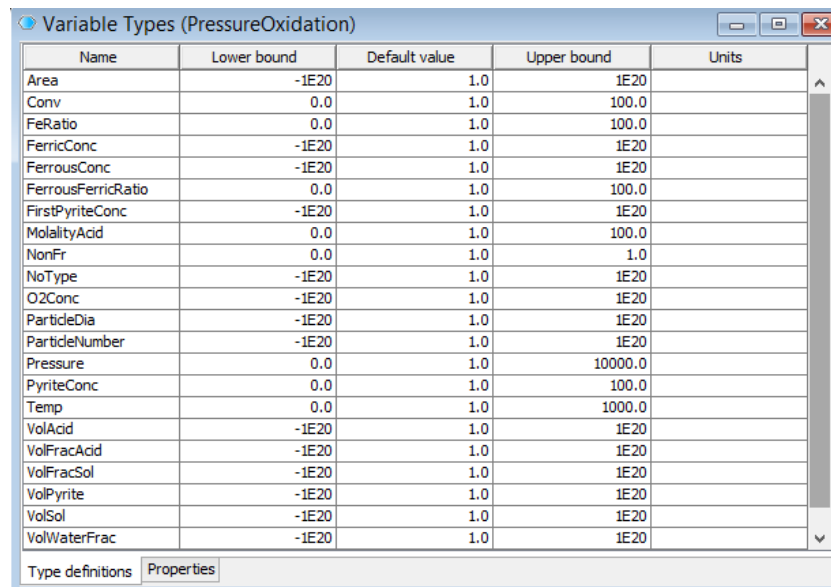
4.1 Modeling and simulation in gPROMS

The leaching processes discussed earlier have been modeled by making use of gPROMS Model builder version 4.1.

The steps involved in carrying out the parameter estimation in gPROMS are as follows:

- Model variables definition

  The model variables involved in the leaching process are defined under the variables tab. Each variable is assigned a name and the lower and upper limits are specified.

Name	Lower bound	Default value	Upper bound	Units
Area	-1E20	1.0	1E20	
Conv	0.0	1.0	100.0	
FeRatio	0.0	1.0	100.0	
FerricConc	-1E20	1.0	1E20	
FerrousConc	-1E20	1.0	1E20	
FerrousFerricRatio	0.0	1.0	100.0	
FirstPyriteConc	-1E20	1.0	1E20	
MolalityAcid	0.0	1.0	100.0	
NonFr	0.0	1.0	1.0	
NoType	-1E20	1.0	1E20	
O2Conc	-1E20	1.0	1E20	
ParticleDia	-1E20	1.0	1E20	
ParticleNumber	-1E20	1.0	1E20	
Pressure	0.0	1.0	10000.0	
PyriteConc	0.0	1.0	100.0	
Temp	0.0	1.0	1000.0	
VolAcid	-1E20	1.0	1E20	
VolFracAcid	-1E20	1.0	1E20	
VolFracSol	-1E20	1.0	1E20	
VolPyrite	-1E20	1.0	1E20	
VolSol	-1E20	1.0	1E20	
VolWaterFrac	-1E20	1.0	1E20	

Figure 7. Variable definition in gPROMS (high pressure pyrite oxidation)

- Model definition

  Under the model tab, the leaching process model is defined as per the syntax allowed in gPROMS. It involves specifying the names of the parameters, variables and kinetic

equations involved in the leaching process. The model defined for each leaching case are shown in Appendices I, II and III respectively.

- Process definition

  Once the leaching process model has been defined, the process tab is selected and in each case, a process definition is done. It involves assigning values for the parameters and variables taking part in the leaching process. Also the initial values for the differential equations are specified. The process definition for each leaching case have been shown in Appendices I, II and III respectively.

- Experimental data input

  The experiment tab is selected and each experiment is defined separately. The process control actions for the variables affecting the outcome of the experiment are specified within the control tab.

Figure 8. Experiment definition in gPROMS (high pressure pyrite oxidation)

43

- Parameter estimation

Under the parameter estimation tab, the parameters that need to be estimated are specified. For each parameter, the initial value and the corresponding limits are specified. The experiments defined are then included within the estimation within the experiments and measurements tab.

For each experiment, there is a need to specify a variance model. Since parameter estimation is based on the least squares approach, the constant variance model is selected. The parameter estimation model is then executed by selecting the estimate tab.

PARAMETER ESTIMATION PRESSUREOXIDATIONREACTOR (PressureOxid...

Parameter to be estimated	Initial guess	Fixed?	Lower bound	Upper bound
C101.E1	46900.0	☐	10000.0	100000.0
C101.E2	41400.0	☐	10000.0	500000.0
C101.E3	134000.0	☐	10000.0	250000.0
C101.Fpre	0.3	☐	0.3	0.7
C101.K1m	0.0279	☐	0.02	1.0
C101.K2m	0.00269	☐	1E-4	0.005
C101.K3m	8.41E-5	☐	1E-6	2E-4
C101.N1	0.503	☐	0.0	1.0
<new>				

To estimate:
8 physical model parameters, and 9 variance model parameters.

Experiments & measurements | Parameters to be estimated | gPROMS language | Properties

Figure 9. Parameter estimation in gPROMS (high pressure pyrite oxidation)

4.2 Case 1: high pressure pyrite oxidation

4.2.1 Model assumptions

The assumptions made in the modeling of high pressure pyrite oxidation process are as follows:

- The model is assumed to be pseudo-homogeneous as the solids are considered to be in a pseudo-homogeneous phase. It does not include the effect of size distribution of particles. Particle population balances are not included.

- On the basis of the shrinking core model, the particle core shrinkage can be represented in terms of the following equation:

$$\left(\frac{d_i}{d_0}\right)^3 = 1 - X_{FeS_2} \tag{5}$$

  Where,

  d_i inner particle diameter, m

  d_0 outer particle diameter, m

  X_{FeS_2} conversion of pyrite, %

- The pyrite reaction can be represented as the surface reaction that occurs between:
  - Oxygen and pyrite
  - Ferric Ions and pyrite

- The reaction kinetics has a dependence on the concentrations of pyrite, dissolved oxygen, ferric ions, ferrous ions and conversion of pyrite.

- There is passivation which occurs on the surface of the mineral due to elemental sulphur. The passivation term $\left(1 - X_{FeS_2}\right)^{n_1}$ which takes into consideration all the negative

effects of passivation on the rate of pyrite oxidation as the reaction takes place. The parameter n_1 is an experimental parameter that describes the extent of passivation.

- The oxidation (R3) of ferrous ions (Fe^{2+}) back to ferric ion (Fe^{3+}) is considered as a bulk phase reaction and the surface concentration of pyrite at the reactive surface is assumed to remain unchanged as the reaction proceeds.

- Arrhenius equation is used to describe the surface and bulk reaction rate dependency on temperature.

4.2.2 Reaction kinetics

The kinetic model described consists of differential equations to represent the pyrite oxidation reaction rate. The surface reaction that occurs between pyrite and oxygen and pyrite and ferric ions can be described by Equations (10) and (12), respectively.

$$r_1 = k_1 c_{FeS_2,0} \left(\frac{1-X_{FeS_2}}{X_{FeS_2,mean}}\right)^{n_1} \left(\frac{c_{O_2}}{c_{O_2,mean}}\right)^{n_2} \tag{10}$$

$$k_1 = k_{1,mean} \, exp\left(-\frac{E_1}{R}\left(\frac{1}{T} - \frac{1}{T_{mean}}\right)\right) \tag{11}$$

$$r_2 = k_2 c_{FeS_2,0} \left(\frac{1-X_{FeS_2}}{X_{FeS_2,mean}}\right)^{n_1} \left(\frac{c_{Fe^{3+}}}{c_{Fe^{3+},mean}}\right)^{n_3} \tag{12}$$

$$k_2 = k_{2,mean} \, exp\left(-\frac{E_2}{R}\left(\frac{1}{T} - \frac{1}{T_{mean}}\right)\right) \tag{13}$$

Where,

$c_{FeS_2,0}$ initial pyrite concentration, mol m^{-3}

c_{O_2} dissolved oxygen concentration, mol m^{-3}

$c_{O_2,mean}$ mean dissolved oxygen concentration, mol m^{-3}

$c_{Fe^{3+},mean}$ mean concentration of ferric ions, mol m^{-3}

X_{FeS_2} conversion of pyrite, %

$X_{FeS_2,mean}$ mean pyrite conversion, %

r_1 surface reaction rate between pyrite and oxygen, mol m^{-2} min^{-1}

r_2 surface reaction rate between pyrite and ferric ions, mol m^{-2} min^{-1}

k_1 rate constant for pyrite oxidation, -

$k_{1,mean}$ rate constant for pyrite oxidation at mean temperature, mol m^{-2} s^{-1}-

k_2 rate constant for reaction between pyrite and ferric ions, -

$k_{2,mean}$ rate constant for ferric iron oxidation at mean temperature, mol m^{-2} s^{-1}

E_1 activation energy, kJ mol^{-1}

E_2 activation energy, kJ mol^{-1}

n_1 parameter describing surface passivation, -

n_2 dissolved oxygen reaction order, -

n_3 ferric ions reaction order, -

The dissolved oxygen concentration at saturation point $\left(c_{O_2}^*\right)$ can be evaluated from the partial pressure of oxygen (Zhukov et al., 2015).

$$c_{O_2}^* = 101.325\psi\, exp\left(\frac{-0.046T^2+203.357\ln(T/298)-(299.378+0.092T)(T-298)-20591}{8.3143T}\right) P_{O_2} \qquad (14)$$

The factor ψ depends on the molal concentration of sulphuric acid and can be calculated as follows:

$$\psi = \left(\frac{1}{1+2.01628\,[H_2SO_4]}\right)^{0.168954} \qquad (15)$$

Where,

T Temperature, K

P_{O_2} oxygen partial pressure, kPa

$[H_2SO_4]$ molal concentration of sulphuric acid, mol kg^{-1}

In order to improve the parameter estimation, the conversion of pyrite and the concentration of reagents are divided by their mean values as shown in Table 5.

Table 5. Mean values of parameters (Zhukov et al., 2015)

Parameter	Unit	Value
$X_{FeS_2,mean}$	%	50
$c_{L,O_2,mean}$	mol m^{-3}	1E-5
$c_{Fe^{2+},mean}$	mol m^{-3}	1E-6
$c_{Fe^{3+},mean}$	mol m^{-3}	2.5E-6
T_{mean}	^{0}C	210

The oxidation of ferrous ions to ferric ions in the liquid phase can be represented as shown in Equation (16).

$$r_3 = k_3 \left(\frac{c_{Fe^{2+}}}{c_{Fe^{2+},mean}} \right)^{n_4} \left(\frac{c_{O_2}}{c_{O_2,mean}} \right)^{n_5} \tag{16}$$

$$k_3 = k_{3,mean} \, exp\left(-\frac{E_3}{R}\left(\frac{1}{T} - \frac{1}{T_{mean}} \right) \right) \tag{17}$$

Where,

r_3 reaction rate for reaction between ferrous iron and oxygen, mol m^{-3} s^{-1}

k_3 reaction rate constant for ferrous iron oxidation, -

$k_{3,mean}$ rate constant for ferrous iron oxidation at mean temperature, mol m^{-2} s^{-1}

E_3 activation energy, kJ mol^{-1}

$c_{Fe^{2+},mean}$ mean ferrous iron concentration, mol m^{-3}

n_4 ferrous ions reaction order, -

n_5 dissolved oxygen reaction order (reaction R3), -

The rate of backward reaction is given by the following equation:

$$r_{-3} = \frac{r_3}{K_{eq}} \tag{18}$$

Where,

r_{-3} backward reaction (ferric iron to ferrous iron) rate, mol m^{-3} s^{-1}

K_{eq} equilibrium rate constant, -

Considering a typical batch reactor, the mass balance equation in differential form is written as follows:

$$\frac{dX_{FeS_2}}{dt} = \frac{(r_1 + r_2)A_i n}{c_{FeS_2,0}} \tag{19}$$

Where,

A_i particle reactive surface area, m^2

n number of particles per liter of slurry in the reactor, m^{-1}

The rate of ferrous iron production can be represented by Equation (20).

$$\frac{dc_{Fe^{2+}}}{dt} = 15r_2 \frac{A_i n}{\varepsilon} - r_3 + r_{-3} \tag{20}$$

Where,

ε volume liquid fraction in the slurry, m^3 m^{-3} slurry

The rate of ferric iron production can be represented by Equation (21).

$$\frac{dc_{Fe^{3+}}}{dt} = r_1 \frac{A_i n}{\varepsilon} - 14r_2 \frac{A_i n}{\varepsilon} + r_3 - r_{-3} \tag{21}$$

As per the shrinking core model, the size of the particle and the active surface area decreases continuously as the reaction carries on.

Based on the conversion of pyrite, the particle surface area is calculated as shown in Equation (22).

$$A_i = \pi(1 - X_{FeS_2})^{2/3} d_0^2 \tag{22}$$

Where,

d_0 outer particle diameter, m

4.2.3 Experimental data

The kinetic modeling has been done based on the experiments carried out by Long and Dixon (2004) in which pyrite oxidation process was conducted in a laboratory scale autoclave in the presence of high pressure and acidic conditions. The experiments were conducted using massive high grade pyrite from Zacatecas in Mexico. The pyrite samples had a purity of 97 ± 1% and the sulphur to iron molar ratio was found to be 1.92. The process conditions have been summarized in Table 6.

Table 6. Pressure oxidation experimental conditions (Long and Dixon, 2004)

Process parameter	Parameter value
Rotating speed, 1/min	650-950
Reactor temperature, ^{0}C	170-230
Particle mean size, µm	49-125
Partial pressure of oxygen, kPa	320-1035
Density of pulp (pyrite), g/L	1-20
Concentration of sulphuric acid, M	0.5
Reactor configuration	2-L titanium autoclave

The experimental data consists of ten experiments as summarized in Table 7.

Table 7. Experiment summary (Long and Dixon, 2004)

Experiment No.	T (^{0}C)	d_i (μm)	Po_2 (kPa)	m_{FeS_2} (kg/m³)
1	170	62.6	690	1
2	190	62.6	690	1
3	210	48.2	690	1
4	210	62.6	345	1
5	210	62.6	690	1
6	210	62.6	1035	1
7	210	88.1	690	1
8	210	125.1	690	1
9	230	62.6	690	1
10	210	62.6	690	20

4.2.4 Model framework

The high pressure pyrite oxidation leaching process is modeled and simulated in gPROMS and the reaction kinetic parameters are estimated. The model framework along with the estimated parameter values is shown in Table 8.

For the leaching process model implemented in gPROMS, the goodness of the fit is determined by making use of the R^2 value:

$$R^2 = 1 - \frac{\sum(y_i - f(x_i,b))^2}{\sum(y_i - \bar{y})^2} \tag{23}$$

The standard error is calculated as follows:

$$STDErr = \sqrt{\frac{\sum(y_i - f(x_i,b))^2}{N-n}} \tag{24}$$

Where,

y_i experimental data values

$f(x_i, b)$ model predicted values

N number of experimental samples

n number of estimated parameter

Table 8. Model framework for high pressure pyrite oxidation

Framework of the model	Parameter estimation result	
	Model parameter	Value
$\dfrac{dX_{FeS_2}}{dt} = \dfrac{(r_1 + r_2)A_i n}{c_{FeS_2,0}}$		
	E_1, J/mol	39063.30
$\dfrac{dc_{Fe^{2+}}}{dt} = 15r_2 \dfrac{A_i n}{\varepsilon} - r_3 + r_{-3}$	E_2, J/mol	58271.40
$\dfrac{dc_{Fe^{3+}}}{dt} = r_1 \dfrac{A_i n}{\varepsilon} - 14r_2 \dfrac{A_i n}{\varepsilon} + r_3 - r_{-3}$	E_3, J/mol	141896
	f_{Pre}	0.564
$r_1 = k_1 c_{FeS_2,0} \left(\dfrac{1-X_{FeS_2}}{X_{FeS_2,mean}}\right)^{n_1} \left(\dfrac{c_{O_2}}{c_{O_2,mean}}\right)^{n_2}$, where $k_1 = k_{1,mean}\, exp\left(-\dfrac{E_1}{R}\left(\dfrac{1}{T} - \dfrac{1}{T_{mean}}\right)\right)$	$k_{1,\,mean}$, mol/m^2 s	0.0269
	$k_{2,\,mean}$, mol/m^2 s	0.003617
$r_2 = k_2 c_{FeS_2,0} \left(\dfrac{1-X_{FeS_2}}{X_{FeS_2,mean}}\right)^{n_1} \left(\dfrac{c_{O_2}}{c_{Fe^{3+},mean}}\right)^{n_3}$, where $k_2 = k_{2,mean}\, exp\left(-\dfrac{E_2}{R}\left(\dfrac{1}{T} - \dfrac{1}{T_{mean}}\right)\right)$	$k_{3,\,mean}$, mol/m^2 s	0.000179
	n_1	0.319
$r_3 = k_3 \left(\dfrac{c_{Fe^{2+}}}{c_{Fe^{2+},mean}}\right)^{n_4} \left(\dfrac{c_{L,O_2}}{c_{O_2,mean}}\right)^{n_5}$, where $k_3 = k_{3,mean}\, exp\left(-\dfrac{E_3}{R}\left(\dfrac{1}{T} - \dfrac{1}{T_{mean}}\right)\right)$	Goodness of fit	
$r_{-3} = \dfrac{r_3}{K_{eq}}$	Standard error	0.03012
	R^2	0.9928

4.2.4 Model predictions

The model predictions for the high pressure pyrite oxidation process are shown in Figure 10.
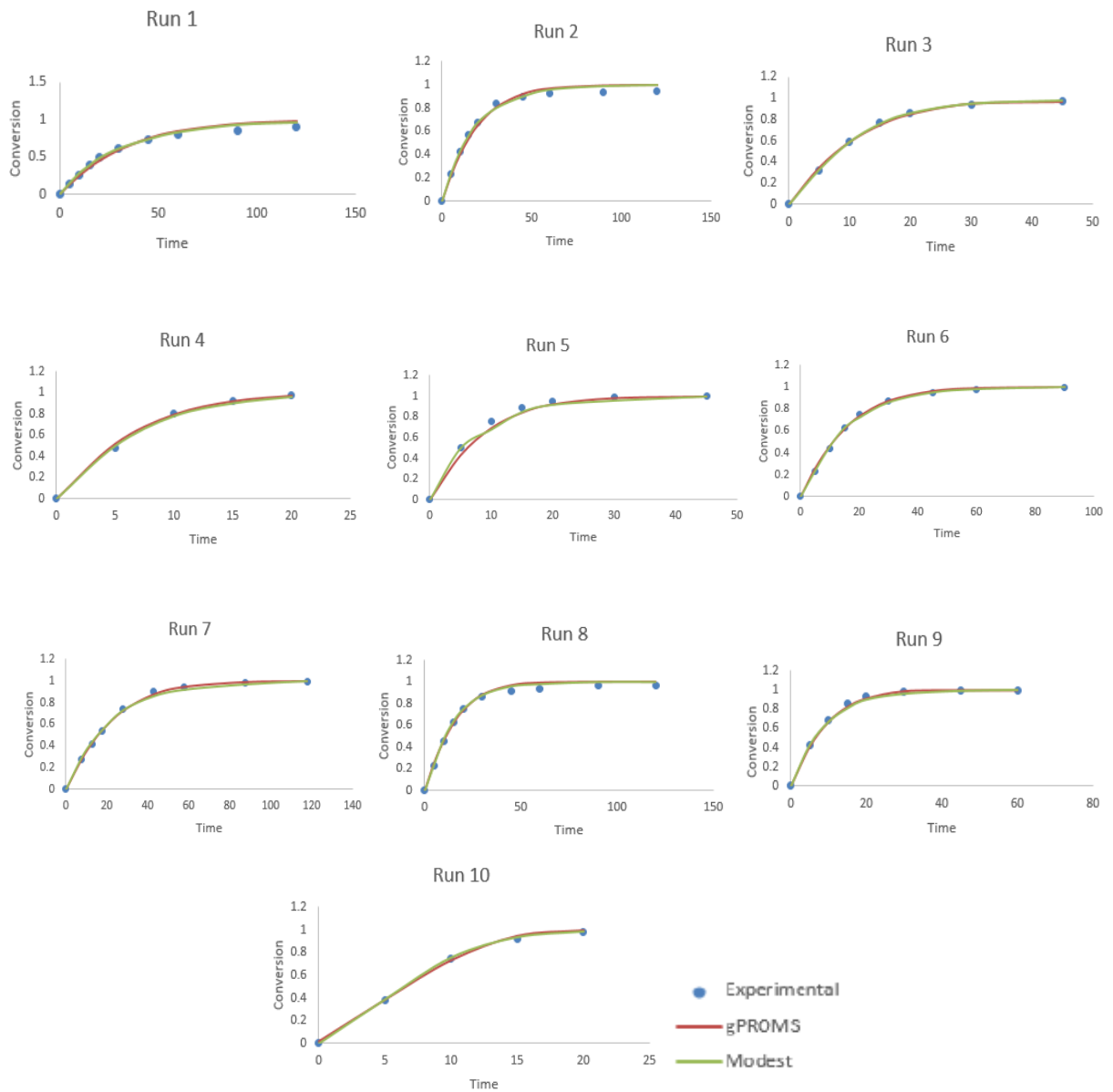
Figure 10. Model predictions (conversion vs time) high pressure pyrite oxidation

4.3 Case 2: Direct oxidation zinc concentrate leaching

4.3.1 Model assumptions

The assumptions made in the modeling of zinc concentrate leaching process are as follows:

- The kinetic model is developed on the basis of the traditional shrinking core model and takes into consideration the reactions that occur at the reacting concentrate surface between ZnS (sphalerite) and the respective oxidizing agents (oxygen and ferric iron), particle diffusion and the subsequent decrease in active surface area as the reaction proceeds.

- The model assumes that pseudo steady state conditions prevail in which there is no time dependence of the oxidant concentration profile because of long residence times within the reactor.

- The concentration of zinc at the particle surface is assumed to be constant and by the mineralogy of the concentrate, the leaching rate of iron is assumed to be the same as that for zinc leaching.

- It is assumed that there are no reactions occurring within the pores of the particles.

4.3.2 Reaction kinetics

4.3.2.1 Oxidation using oxygen

Xie et al. (2007) proposed that the oxidation and leaching reaction takes place by oxidation in the presence of oxygen. The additional ferrous iron serves as a catalyst and increases the rate of oxidation. The leaching reaction occurs according to the shrinking core model as shown in Figure 6. As the reaction takes place, on the reactive surface layer, a passive layer is formed that

gradually increases in its thickness. During the oxidation reaction (R9), oxygen acts as a limiting reagent and diffuses through the passive layer into the particle surface where the leaching reaction occurs.
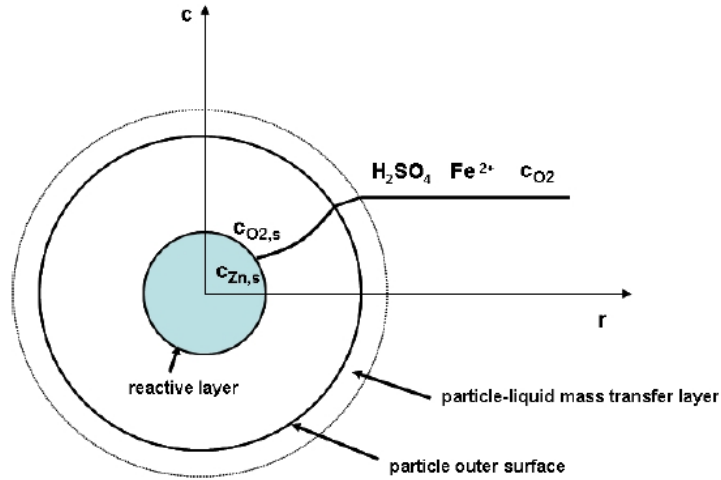
Figure 11. Shrinking core model for zinc concentrate leaching

The zinc leaching reaction is considered to be a surface reaction and the concentration of zinc at the solid particle surface is assumed to be constant. The surface reaction rate is:

$$r_4 = k_s c_{Zn,s} c_{O_{2,s}}^{n_6} c_{H_2SO_4}^{n_7}(1 + bc_{Fe^{2+}}) = k_4 c_{O_{2,s}}^{n_6} c_{H_2SO_4}^{n_7}(1 + bc_{Fe^{2+}}) \tag{25}$$

Where,

r_4 reaction rate at the surface for zinc oxidation by oxygen, mol m^{-2} min^{-1}

k_s reaction rate constant, -

k_4 reaction rate constant, -

$c_{Zn,s}$ concentration of zinc at the surface in solids, mol m^{-3}

$c_{O_{2,s}}$ concentration of dissolved oxygen at the reaction surface, mol m^{-3}

$c_{H_2SO_4}$ sulfuric acid concentration in liquid, mol m^{-3}

n_6 oxygen reaction order, -

n_7 sulfuric acid reaction order, -

b experimental parameter, m^3 mol^{-1}

$c_{Fe^{2+}}$ ferrous iron concentration, mol m^{-3}

The effect of ferrous iron as a catalyst is taken into consideration by applying a simple linear factor to the rate equation. On the basis of the minerology of the concentrate, it is assumed that the iron leaching from the particles takes place at the same rate as Zinc leaching.

The rate of dissolution can now be written as follows:

$$\frac{dc_{Zn}}{dt} = -r_4 A_i n \tag{26}$$

Where,

c_{Zn} zinc concentration in solids, mol m^{-3}

A_i reacting particle surface area, m^2

n number of particles within the reactor, m^{-3}

The surface oxygen concentration $c_{O_{2,s}}$ is obtained numerically from mass balance. Pseudo steady state conditions are assumed inside the particle and as a result the oxygen concentration profile inside the particles is independent of time.

At steady state, the concentration profile in case of diffusion through a spherical layer can be shown by Equation (27).

$$c = \frac{c_i (r_o - r)r_i + c_o(r - r_i)r_o}{r(r_o - r_i)} \tag{27}$$

The concentration gradient in the layer can then be written as shown in Equation (28).

$$\frac{dc}{dr} = \frac{r_i r_o (c_o - c_i)}{(r_o - r_i)r^2} \tag{28}$$

Where,

r_i reaction surface radius, m

r_o outer particle surface radius, m

c_i concentration at the inner particle surface, mol m^{-3}

c_o concentration at the outer particle surface, mol m^{-3}

The rate of diffusion can be calculated for either the inner or the outer surface of the layer by making use of the concentration gradient and the coefficient of diffusion.

$$\dot{n}_{o_2} = -D_e A_r \frac{dc}{dr} = -D_e A_r \frac{r_0\left(c_{O_2}-c_{O_2,s}\right)}{(r_0-r_i)r_i} = -D_e A_r \frac{r_i\left(c_{O_2}-c_{O_2,s}\right)}{(r_0-r_i)r_0} \tag{29}$$

Where,

D_e effective particle diffusivity, m^2 min^{-1}

A_r surface area of layer, m^2

c_{O_2} concentration of dissolved oxygen, mol m^{-3}

The oxygen mass balance for the reacting surface can then be written as shown in Equation (30).

$$f = 2k_i c_{O_2,s}^{n_6} c_{H_2SO_4}^7 (1 + bc_{Fe^{2+}})a_i - D_e a_o \frac{r_i\left(c_O-c_{O_2,s}\right)}{(r_0-r_i)r_0} = 0 \tag{30}$$

Where,

k_i reaction rate constant, -

a_i inner particle surface area, m^2

a_0 outer particle surface area, m^2

Due to lack of information about the concentration of dissolved oxygen in the autoclave reactor and also on account of the high stirring speed, it is assumed that the oxygen level is at saturation

and depends only on the oxygen partial pressure. The concentration of dissolved oxygen is obtained from the partial pressure of oxygen.

$$c_{O_2}^* = K_{O_2} p_{O_2}$$ (31)

Where,

$c_{O_2}^*$ concentration of dissolved oxygen at saturation, mol m^{-3}

K_{O_2} equilibrium constant for oxygen, mol m^{-3} Pa^{-1}

p_{O_2} partial pressure of oxygen, Pa

For the parameter estimation case, the equilibrium constant for oxygen is taken as 0.4 mol/m^3 kPa at 100 ^{0}C as reported by Kaskiala (2005).

The dependence of the rate of reaction on the temperature is taken into consideration by making use of the Arrhenius equation. To improve parameter estimation, the Arrhenius equation is used in its modified form as shown below.

$$k_4 = k_{4,mean} exp\left(-\frac{E_4}{R}\left(\frac{1}{T} - \frac{1}{T_{mean}}\right)\right)$$ (32)

$$k_5 = k_{5,mean} exp\left(-\frac{E_5}{R}\left(\frac{1}{T} - \frac{1}{T_{mean}}\right)\right)$$ (33)

Where,

$k_{4,mean}$ rate constant at mean temperature, mol m^{-2} s^{-1}

$k_{5,mean}$ rate constant at mean temperature, mol m^{-2} s^{-1}

k_5 reaction rate constant, -

E_4 activation energy, J mol^{-1}

E_5 activation energy, J mol^{-1}

R gas constant, 0.008314 kJ mol^{-1} K^{-1}

4.3.2.2 Oxidation using ferric iron

In case of this mechanism, again the shrinking core model is utilized and the oxygen and ferric iron concentrations are iteratively solved using Eq. (30). The leaching reaction is assumed to proceed by ferric iron oxidation (R11).

$$r_5 = k_5 c_{Fe^{3+},s}^{n_8} c_{H_2SO_4}^{n_9} \tag{34}$$

Where,

r_5 reaction rate at the surface for zinc oxidation by ferric iron (Fe^{3+}), mol m^{-2} min^{-1}

n_8 reaction order for ferric, -

n_9 reaction order for sulphuric acid, -

$c_{Fe^{3+},s}$ ferric iron concentration at the reactive surface, mol m^{-3}

At the same time, there is also oxidation that takes place by molecular oxygen (R9).

$$r_4 = k_4 c_{O_{2,s}}^{n_6} c_{H_2SO_4}^{n_7} \tag{35}$$

The total rate of leaching can be taken as the sum of the Equations (34) and (35)

$$\frac{dc_{Zn}}{dt} = -(r_4 + r_5)A_i n \tag{36}$$

It is assumed that the iron present in the concentrate has the same leaching rate as that of zinc. By incorporating the relative amount of Zn (zinc) and Fe (iron) present in the ore sample, the overall iron leaching rate can be calculated as follows:

$$\frac{dc_{Fe}}{dt} = -\frac{m_{f,Fe}}{m_{f,Zn}} (r_4 + r_5)A_i n \tag{37}$$

Where,

$m_{f,Fe}$ mass fraction of Fe in ore, %

$m_{f,Zn}$ mass fraction of Zn in ore, %

From the reaction R1, it can be seen that iron gets leached as ferrous ion and also ferrous iron from reaction R2, is produced by the reaction of zinc with ferric iron. In solution, the ferrous iron undergoes oxidation to ferric iron (Fe^{3+}) in the presence of molecular oxygen. The reaction reported by Verbaan and Grundwell (1986) for the ferrous ion oxidation is as follows.

$$r_6 = k_6 e^{\left(\frac{-E_6}{RT}\right)} c_{Fe^{2+}}^2 c_{O_2} c_{H^+}^{-0.35} \tag{38}$$

Where,

r_6 reaction rate for ferrous ion oxidation to ferric ions, mol m^{-2} min^{-1}

k_6 reaction rate constant, -

E_6 activation energy, kJ mol^{-1}

c_{H^+} hydrogen ion (H^+) concentration in liquid, mol m^{-3}

For the liquid bulk phase, the ferrous iron kinetic equation can be considered as follows.

$$\frac{dc_{Fe^{2+}}}{dt} = \frac{m_{f,Fe}}{m_{f,Zn}} (r_4 + r_5) A_i n + 2 r_5 A_i n - r_6 \tag{39}$$

Similarly, the following kinetic equation can be written for ferric iron.

$$\frac{dc_{Fe^{3+}}}{dt} = -2 r_5 A_i n + r_6 \tag{40}$$

4.3.3 Experimental data

The zinc leaching model is based on the experimental work carried out by Xie et al. (2007). In their study, batch experiments were carried out in an autoclave under different experimental conditions. The temperature, the average particle size, the partial pressure of oxygen and sulphuric acid concentration and initial ferrous iron concentration was varied for each experimental run as shown in Table 9. The concentrate used by Xie et al. (2007) for the leaching batch experiments comprises of 40.85 % Zn (zinc), 1.41 % Cu (copper), 15.21 % Fe (iron) and 31.67 % S (sulphur). The experiments were done in an autoclave of volume 2 dm^3 and the stirring speed was maintained at 600 min^{-1}.

Table 9. Experimental data (Xie et al., 2007)

Experimental Run	dp, μm	T, ^{0}C	p_{O_2} , Mpa	H_2SO_4, g dm^{-3}	Fe^{2+}, mol m^{-3}
1	44.7	140	1.4	50	0
2	77.7	140	1.4	50	0
3	101.3	140	1.4	50	0
4	150.7	140	1.4	50	0
5	77.7	120	1.4	50	0
6	77.7	130	1.4	50	0
7	77.7	140	1.4	50	0
8	77.7	150	1.4	50	0
9	77.7	140	0.8	50	0
10	77.7	140	1.0	50	0
11	77.7	140	1.1	50	0
12	77.7	140	1.2	50	0
13	77.7	140	1.4	50	0
14	77.7	140	1.4	50	0
15	77.7	140	1.4	50	0
16	77.7	140	1.4	50	0
17	77.7	140	1.4	70	0
18	77.7	140	1.4	100	0
19	77.7	140	1.4	50	0
20	77.7	140	1.4	50	0.00825
21	77.7	140	1.4	50	0.01900
22	77.7	140	1.4	50	0,03851

4.3.4 Model framework
The model framework along with the estimated parameter values is shown in Table 10.

Table 10. Model framework for zinc concentrate leaching

Framework of the model	Parameter estimation result	
	Model parameter	Value

Framework of the model	Model parameter	Value
$$\frac{dc_{Zn}}{dt} = -(r_4 + r_5)A_i n$$ $$\frac{dc_{Fe^{2+}}}{dt} = \frac{m_{f,Fe}}{m_{f,Zn}}(r_4 + r_5)A_i n + 2r_5 A_i n - r_6$$ $$\frac{dc_{Fe^{3+}}}{dt} = -2r_5 A_i n + r_6$$ $$\frac{dc_{H_2SO_4}}{dt} = -2r_5 - 2r_6$$ $$r_4 = k_4 c_{O_{2,s}}^{n_6} c_{H_2SO_4}^{n_7}, \text{ where } k_4 = k_{4,mean} exp\left(-\frac{E_4}{R}\left(\frac{1}{T} - \frac{1}{T_{mean}}\right)\right)$$ $$r_5 = k_5 c_{Fe^{3+},s}^{n_8} c_{H_2SO_4}^{n_9}, \text{ where } k_5 = k_{5,mean} exp\left(-\frac{E_5}{R}\left(\frac{1}{T} - \frac{1}{T_{mean}}\right)\right)$$ $$r_6 = k_6 e^{\left(\frac{-E_3}{RT}\right)} c_{Fe^{2+}}^2 c_{O_2} c_{H^+}^{-0.35}$$	E_4, J/mol	56.353E+3
	E_5, J/mol	97.502E+3
	$K_{4, mean}$, mol/m^2 s	8.419E-3
	$K_{5, mean}$, mol/m^2 s	1.243E-7
	D_e, m^2/min	1.455E-9
	n_6	0.638
	Goodness of fit	
	Standard error	0.0528
	R^2	0.935

4.3.5 Model predictions

The model predictions for zinc concentrate leaching process have been shown below in Figure 12.
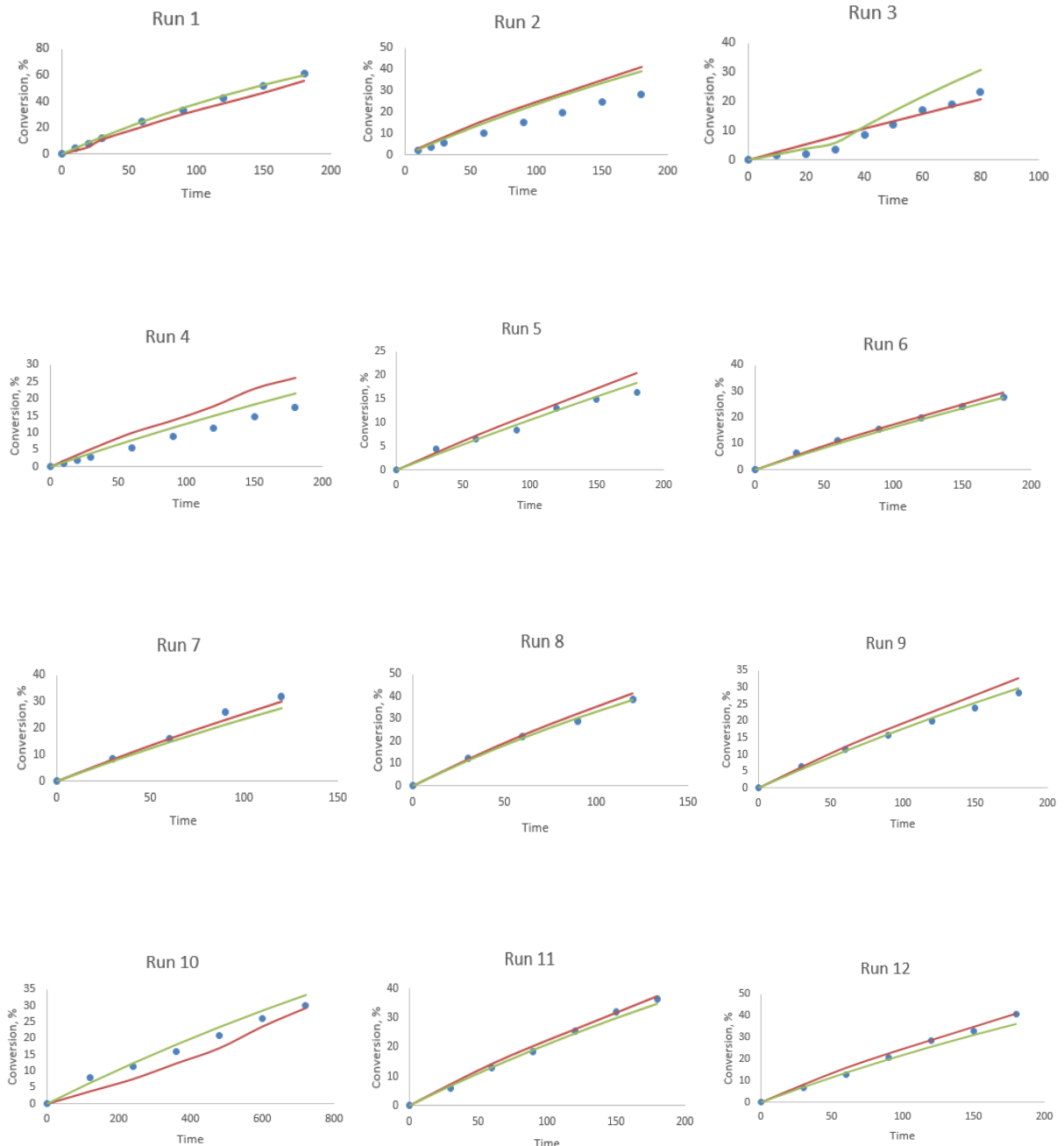
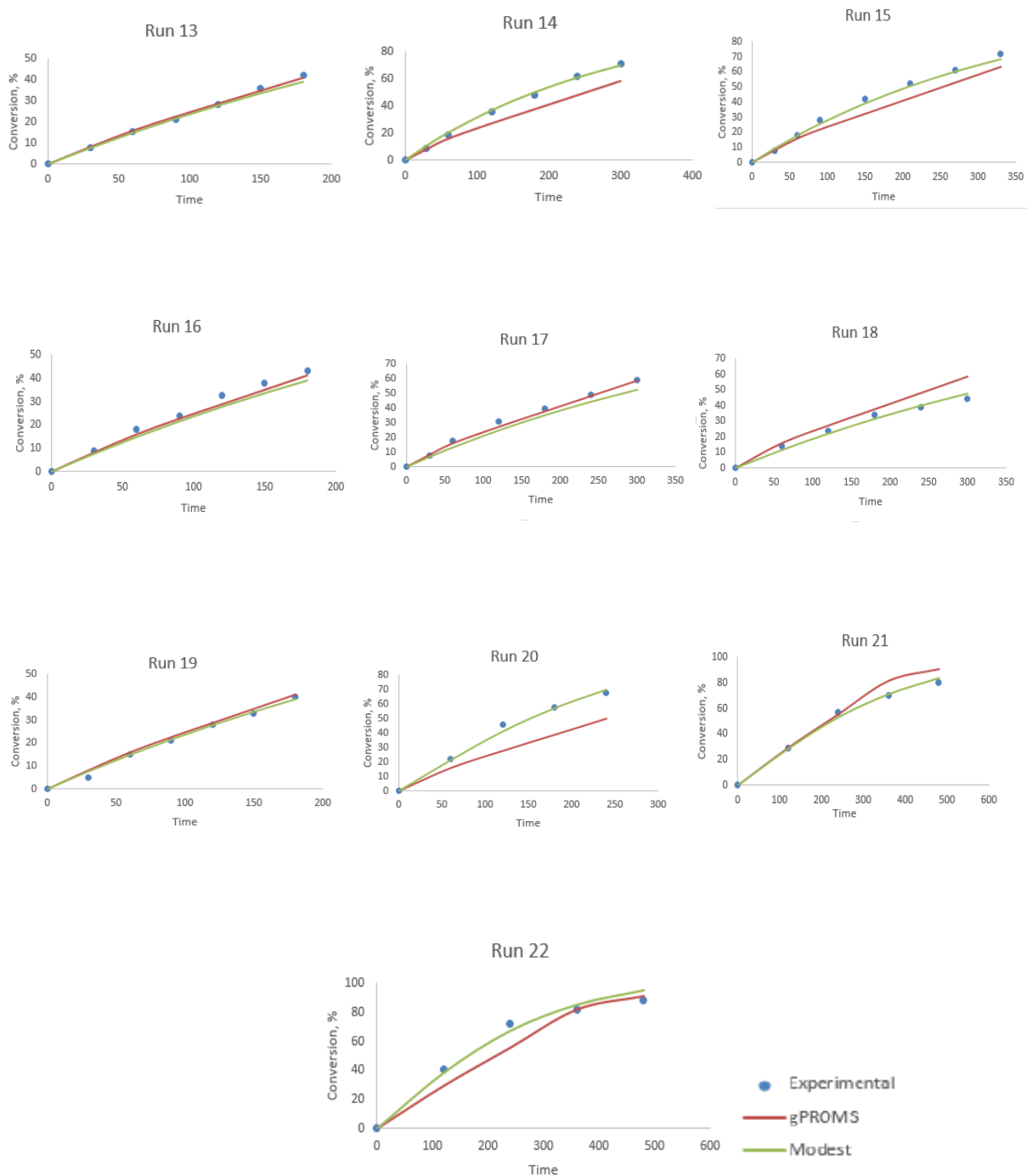Figure 12. Model predictions (conversion vs time) for zinc concentrate leaching

4.4 Case 3: Gold chloride leaching using RDE

4.4.1 Model assumptions

The assumptions made in the modeling of gold chloride leaching process are as follows:

- The mass transfer rate depends on the temperature, concentration of the oxidant and the rotating speed of the electrode.

- The model is implemented as a mixed control system where the gold dissolution rate depends on the surface reaction rate and the mass transfer phenomena on the disc surface.

- The gold leaching from the disc surface is assumed to be an ideal system in comparison to a stirred tank system where there is leaching of particles under non-ideal conditions.

4.4.2 Dissolution model for gold chloride leaching using rotating disc electrode (RDE)

In order to study the mechanisms involved in gold chloride leaching, gold dissolution model has been developed based on experimental study carried out at Aalto University and kinetic modeling done at Lappeenranta University of Technology. The gold dissolution from the rotating disc electrode (RDE) was used in gold oxidation in chloride solution at the disc surface in the presence of oxidizing agents such as Cu^{2+} and Fe^{3+}.

The reaction rate at the surface is described as follows by Equation (41).

$$r_s = kc_s^n \tag{41}$$

Where,

r_s reaction rate at the surface, mol m^2 s^{-1}

k rate constant, -

c_s oxidant concentration at the disc surface, mol m^{-3}

n oxidant reaction order, -

The dependence of the rate constant on temperature can be taken into consideration by applying the Arrhenius equation in its modified form as shown in Equation (42).

$$k = k_{mean} exp\left(-\frac{E}{R}\left(\frac{1}{T} - \frac{1}{T_{mean}}\right)\right)$$
(42)

Where,

k_{mean} reaction rate constant at mean temperature, mol m^{-2} s^{-1}

E activation energy, kJ mol^{-1}

T temperature, K

T_{mean} mean temperature, K

R gas constant, 0.008314 kJ mol^{-1} K^{-1}

A mixed control system can be used to describe the gold dissolution model in which the rate of reaction at the surface and the rate of diffusion has effect on rate of dissolution of gold. The diffusion of the oxidant occurs across the boundary layer to the surface of the disc. Therefore, the rate of mass transfer of oxidant across the boundary layer can be represented in terms of the following equation.

$$r = k_L(c - c_s)$$
(43)

Where,

r mass transfer rate of oxidant across the boundary layer, mol m^2 s^{-1}

k_L mass transfer coefficient across the boundary layer, mol m^2 s^{-1}

c oxidant concentration in bulk liquid, mol m^{-3}

c_s oxidant surface concentration, mol m^{-3}

At steady state, the surface reaction rate (r_s) equals the mass transfer rate (r). As a result the oxidant surface concentration can be obtained by solving Equations (41) and (43).

4.4.3 Experimental data

The experimental data was obtained from gold dissolution experiments carried out using a rotating disc electrode at Aalto University. The experiments were carried out by varying the temperature, the concentration of the oxidants (Cu^{2+} and Fe^{2+}) and the speed of rotation.

The experimental data can be organized in two sets as shown in Tables 11 and 12 respectively: Data set 1.
Oxidant used: Cu^{2+}

Table 11. Experimental data (Cu^{2+} as oxidant)

Experimental Run	c, mol m^{-3}	T, ^{0}C	μ, kg m^{-1} s^{-1}
1	0.5	75	3.78E-04
2	0.5	80	3.46E-04
3	0.5	85	3.34E-04
4	0.5	88	3.14E-04
5	0.5	92	3.00E-04
6	0.5	95	2.98E-04
7	0.02	95	2.98E-04
8	0.10	95	2.98E-04

Data set 2.
Oxidant used: Fe^{3+}

Table 12. Experimental data (Fe^{3+} as oxidant)

Experimental Run	c, mol m^{-3}	T, ^{0}C	μ, kg m^{-1} s^{-1}
1	0.5	65	4.33E-04
2	0.5	75	3.78E-04
3	0.5	85	3.34E-04
4	0.5	95	2.98E-04
5	0.5	95	2.98E-04
6	0.5	95	2.98E-04
7	0.02	95	2.98E-04

4.4.4 Model framework

The model framework along with the estimated parameter values is shown in Table 13.

Table 13. Model framework for gold leaching using RDE

Framework of the model	Parameter estimation result	
$\dfrac{dc_s}{dt} = r_s - r$ $r_s = kc_s^n$, where $k = k_{mean} exp\left(-\dfrac{E}{R}\left(\dfrac{1}{T} - \dfrac{1}{T_{mean}}\right)\right)$ $r = k_L(c - c_s)$, where $k_L = Sh * D$ $Sh = a_1 Re^{a_2} Sc^{1/3}$ $Re = \dfrac{Nd^2}{v}$ $Sc = \dfrac{v}{D}$	Case 1: Fe^{3+} as oxidant	
	Parameter	Value
	E_1, J/mol $K_{1,\ mean}$, g/m^2 s a_1 a_2 n	36925.3 8.529E-5 1.05 1.167 0.293
	Standard error R^2	0.001715 0.9429
	Case 2: Cu^{2+} as oxidant	
	Parameter	Value
	E_1, J/mol $K_{1,\ mean}$, g/m^2 s a_1 a_2 n	79767 1.68E-5 0.350 1.40 0.329
	Standard error R^2	0.0638 0.9175

4.4.5 Model predictions

The model predictions for gold leaching using rotating disc electrode (RDE) in the presence of oxidant Fe^{3+} are shown below in Figure 13.
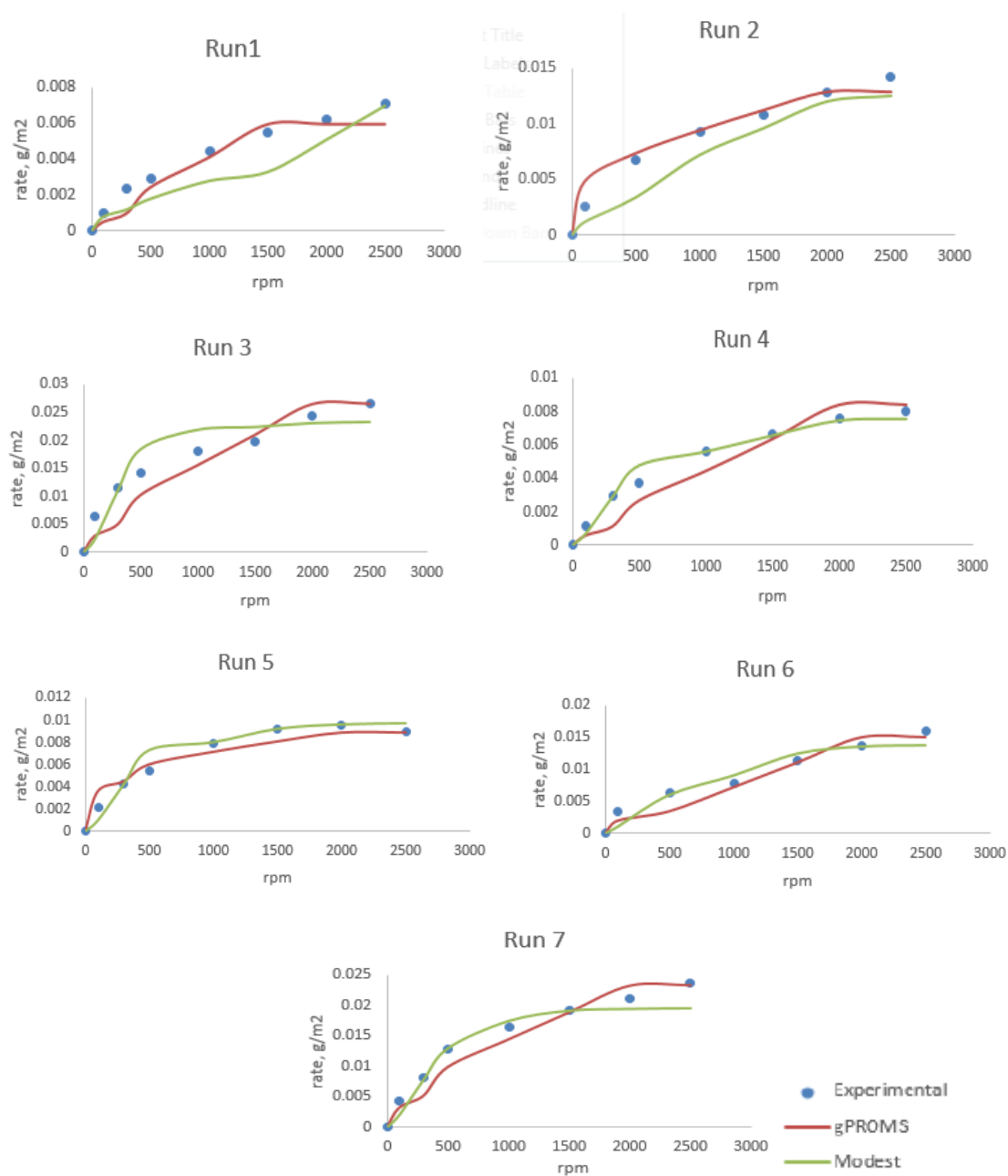

Figure 13.Model predictions (for gold leaching in RDE with Fe^{3+} as oxidant)

The model predictions for gold leaching using rotating disc electrode (RDE) in the presence of oxidant Cu^{2+} have been shown below in Figure 14.
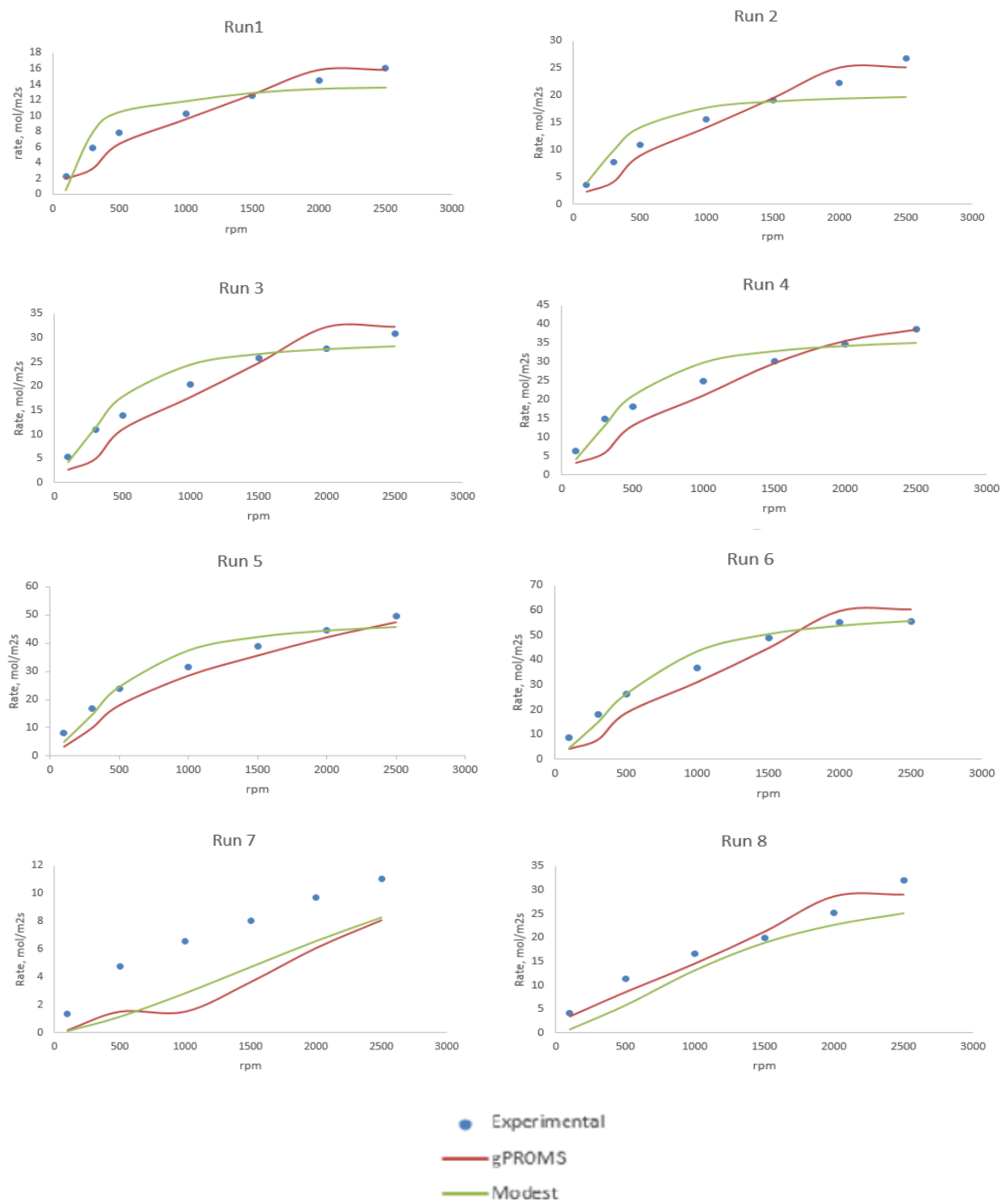

Figure 14. Model predictions (for gold leaching in RDE with Cu^{2+} as oxidant)

4.5 Reactor modeling

Leaching of zinc concentrates is often carried out industrially in autoclaves that are complex multiphase reaction systems. These autoclaves are horizontal and cylindrical reactor vessels consisting of several compartments where the leaching reaction occurs. The compartments are well agitated so as to ensure that the solids remain suspended and there is good dispersion of oxygen. As a result, the autoclave reactor is modeled as continuous stirred tank reactors in series (Baldwin et al. 1995). The objective of this particular study was to fit the estimated kinetic model parameters (Table 10) obtained using gPROMS into process simulation software Aspen Plus (v. 8.6).

4.5.1 Process description

The zinc concentrate feed introduced into the autoclave consists mostly of sulfidic minerals and the zinc dissolution has been expressed in terms of a shrinking core model in which the shrinkage rate is proportional to the concentration of the oxygen dissolved within the system. The configuration of the leaching autoclave reactor (Cominco reactor) is shown in figure 15.
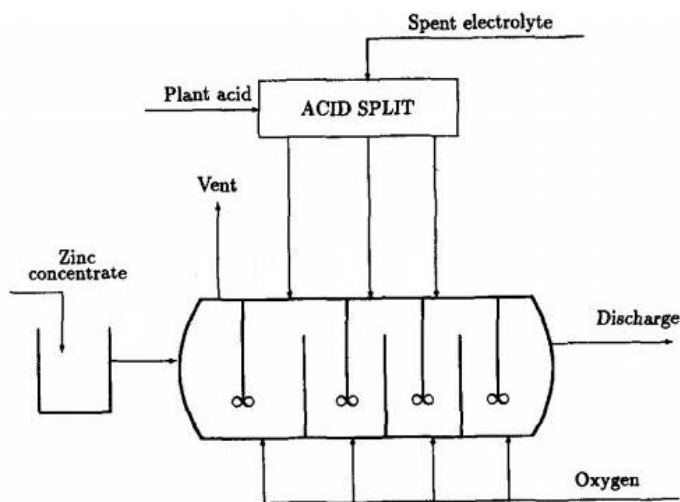

Figure 15. Zinc pressure leaching autoclave reactor (Baldwin et al. 1995)

The autoclave reactor consists of four compartments with the first being slightly larger than the remaining three and the temperature is maintained in the range of 140^0C to 180^0C. The zinc concentrate feed enters the first compartment and is mixed with the spent electrolyte and plant acid that is fed to the first three compartments. In addition to this, all the compartments are well stirred and supplied with sufficient oxygen for the leaching reaction to proceed.

The reactor configuration as discussed above is utilized for modeling the zinc concentrate leaching in the presence of molecular oxygen. The reaction kinetics and the model parameters estimated using gPROMS model builder (Table 10) are used for the reactor simulation. The autoclave reactor has been simulated as a series of continuous stirred tank reactors in Aspen Plus (v. 8.6).

4.5.2 Process simulation conditions

The sphalerite leaching reaction has been shown below:

$$ZnS + 0.5O_2 + H_2SO4 \rightarrow ZnSO_4 + S + H_2O \qquad (R14)$$

The process simulation conditions have been shown in Table 14.

Table 14. Process simulation conditions (Xie et al., 2007)

Parameter	Value
Zinc concentrate (sphalerite) mass flow, kg/h	18
Oxygen mass flow, kg/h	21.6
Oxgen partial pressure, MPa	1.4
Sulphuric acid concentration, mg/L	50
Reactor volume (Baldwin et al. 1995), L	Reactor 1: 10 Reactor 2: 7.5 Reactor 3: 7.5 Reactor 4: 7.5
Reactor temperature, ^{0}C	170
Reaction kinetics 1. Mean temperature, ^{0}C 2. Activation energy (Table 10), J/mol 3. Rate constant at mean temperature, kmol/m^{3}s	 130 56353 0.00517

4.5.3 Simulation flow diagram

The zinc concentrate feed (sphalerite) is introduced into the first continuous stirred reactor and the reaction mixture flows from one reactor to the next. Within each reactor, sulphuric acid with a concentration of 50 mg/L is introduced and there is sufficient oxygen mass flow for the leaching reaction to proceed. The sphalerite conversion is determined at the outlet of the last reactor. The continuous stirred tank reactor model available in the Aspen Plus (v. 8.6) model library is utilized for the simulation. The property method selected is UNIQUAC as it was found to be the most suitable for simulating hydrometallurgical processes. The stream compositions at the outlet of each reactor have been given in Appendix IV.

The simulation flow diagram for the zinc concentrate leaching process has been shown below in figure 16.
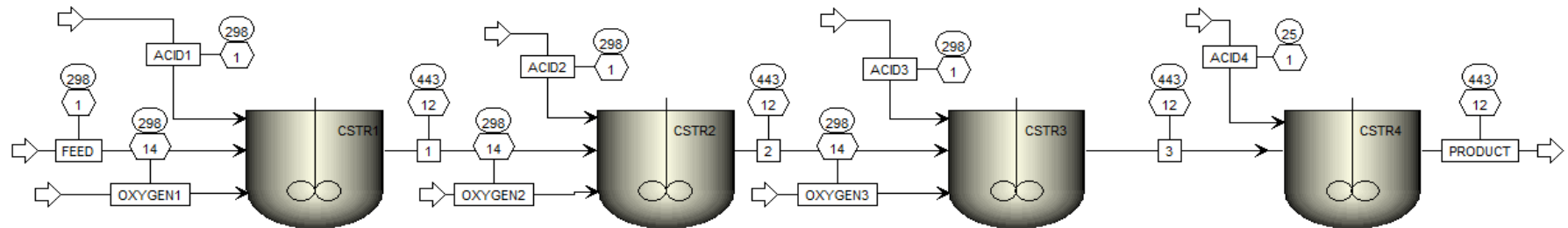

Figure 16. Simulation flow diagram (Aspen Plus v. 8.6)

4.5.4 Results

The zinc concentrate leaching process is simulated in Aspen Plus (v. 8.6) and the result of simulation has been shown below in Table 15.

The sphalerite conversion is calculated at the outlet of reactor number four and is found to be 95.56 percent.

$$Conversion, X = \frac{F_{A_0} - F_A}{F_{A_0}} \tag{45}$$

Where,

F_{A_0} inlet sphalerite mass flow, kg/h.

F_A outlet sphalerite mass flow, kg/h

Table 15. Simulation results for multistage continuous sphalerite oxidation

Reactor Number	Sphalerite outlet mass flow (F_A, kg/h)	Conversion, %
1	12.52	30.44
2	8.42	52.67
3	4.27	76.28
4	0.80	95.56

Sensitivity analysis

The sensitivity analysis is carried out so as to determine the optimum reactor operation temperature and the required oxygen mass flow so as to maximize the conversion. The temperature within the reactor is varied between 140^0C to 180^0C and the oxygen mass flow is varied between 3.6 kg/h to 36 kg/h.
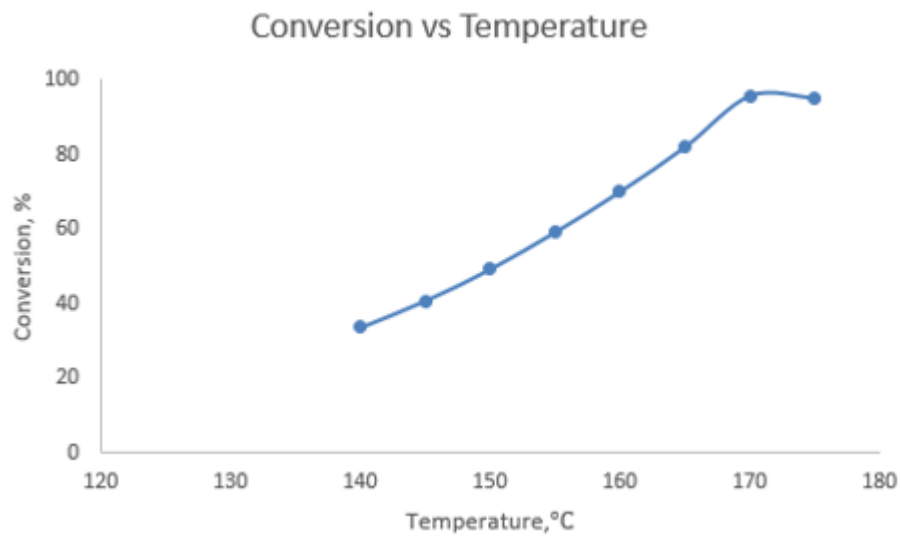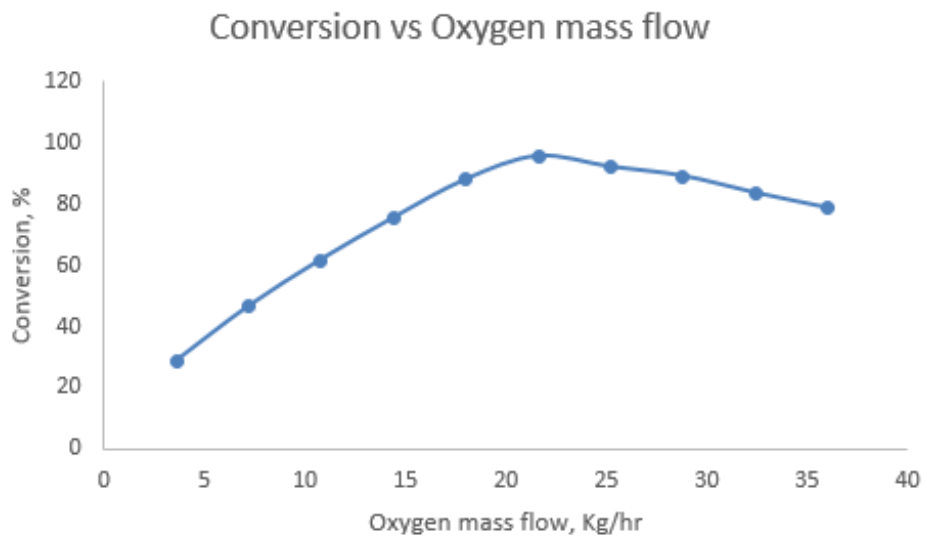
Figure 17. Conversion vs reactor temperature

Figure 18. Conversion vs oxygen mass flow

5 Discussion

The results obtained from the model predictions, the parameter estimation study carried out in gPROMS for the three hydrometallurgical processes (high pressure pyrite oxidation, zinc concentrate leaching and gold chloride leaching using RDE) and the reactor modeling done for the zinc concentrate leaching case in Aspen Plus (v. 8.6) are discussed below:

High pressure pyrite oxidation

For the parameter estimation, the reaction orders n_2, n_3, n_4 and n_5 were fixed as per the values reported in literature and eight parameter values were estimated on the basis of the experimental data used by Long and Dixon (2004) in their experiments. From the model predictions, it is evident that there is good agreement between the experimental and predicted values. The coefficient of fitting is found to be 0.992.

The estimated values for the activation energies E_1 and E_2 are found to be in close accordance with those reported by Long and Dixon (2004) in their study (33.2 kJ/mol). The parameters estimated using gPROMS have been compared with those obtained using the Modest program as shown below in Table 16. It can be observed that the difference in the results obtained by these two software is only marginal.

Table 16. Comparison of estimated parameters (High pressure oxidation)

Model parameter	Estimated value	
	gPROMS	Modest
E_1, J/mol	39063.3	46100
E_2, J/mol	58271.4	50000
E_3, J/mol	14186	109000
f_{Pre}	0.563	0.486
$k_{1, mean}$, mol/m^2 s	0.02685	0.0295
$k_{2, mean}$, mol/m^2 s	0.003617	0.00277
$k_{3, mean}$, mol/m^3 s	0.000179	7.09E-05
n_1	0.319	0.45
Standard error	0.03012	0.02706
R^2	0.9927	0.99418

The correlation matrix is used to evaluate the parameter estimation problem. The possible cross correlation between the estimated parameters can be observed from the correlation matrix produced using gPROMS as shown in Table 17. Parameters with absolute value close to unity (1) indicate a high degree of correlation with each other and vice versa.

Table 17. Correlation matrix (high pressure pyrite oxidation)

Parameter	No.	1	2	3	4	5	6	7	8
E_1	1	1							
E_2	2	0.997	1						
E_3	3	-0.999	-0.999	1					
f_{Pre}	4	0.822	0.807	-0.818	1				
$k_{1, mean}$	5	0.683	0.686	-0.676	0.323	1			
$k_{2, mean}$	6	-0.827	-0.831	0.822	-0.518	-0.971	1		
$k_{3, mean}$	7	-0.63	-0.611	0.626	-0.948	-0.00706	0.218	1	
n_1	8	-0.256	-0.265	0.249	0.15	-0.864	0.731	-0.443	1

In this case, it can be seen that the model parameters E_1, E_2 and E_3 are in close correlation with each other.

Direct oxidation zinc concentrate leaching

From the model predictions, it is evident that the experimental and predicted values are in close agreement with each other. For the parameter estimation, the coefficient of determination was found to be 93.54 % showing reasonably good fitting. The estimated reaction kinetic parameters like activation energies E_1 and E_2 are found to be in close agreement with the values reported by Xie et al (2007) in their experiments.

The parameters estimated using gPROMS have been compared with those obtained using the Modest program as shown below in Table 18. The difference in the results obtained by these two software is only marginal.

Table 18. Comparison of estimated parameters (zinc concentrate leaching)

Model parameter	Estimated value	
	gPROMS	Modest
E_4, J/mol	5.64E+04	6.08E+4
E_5, J/mol	9.75E+04	9.67E+4
$K_{4, mean}$, mol/m^2 s	8.42E-03	7.56E-3
$K_{5, mean}$, mol/m^2 s	1.24E-07	0.47E-7
D_e, m^2/min	1.46E-09	0.91E-9
n_6	0.638	0.638
Standard error	0.0528	0.0284
R^2	0.935	0.981

The correlation matrix is used to evaluate the parameter estimation problem. The possible cross correlation between the estimated parameters can be observed from the correlation matrix produced using gPROMS as shown in Table 19. Parameters with absolute value close to unity (1) indicate a high degree of correlation with each other and vice versa.

Table 19. Correlation matrix (zinc concentrate leaching)

Parameter	No.	1	2	3	4	5	6
E_4	1	1					
E_5	2	0.828	1				
$K_{4, mean}$	3	0.589	0.608	1			
$K_{5, mean}$	4	0.879	0.859	0.809	1		
D_e	5	-0.00546	-0.077	-0.669	-0.171	1	
n_6	6	0.00277	0.0741	0.667	0.167	-1	1

In this case, it can be seen that the model parameters E_4 and $k_{5, mean}$ and E_5 and $k_{5, mean}$ are in correlation with each other to some extent.

Gold chloride leaching using RDE

From the model predictions observed in Figures 15 and 16, it is quite clear that there is good agreement between the experimental and predicted gold dissolution rates. There is model discrepancy observed when the speed of rotation of the disc electrode is quite high (more than 1500 rpm).

The parameters estimated using gPROMS have been compared with those obtained using the Modest program as shown below in Tables 20 and 21 respectively. It can be observed that the difference in the results obtained by these two software is only marginal.

Table 20. Comparison of estimated parameters (gold leaching, Fe^{3+} as oxidant)

Model parameter	Estimated value	
	gPROMS	Modest
E, J/mol	3.69E+4	3.91E+4
k_{mean}, g/m^2 s	8.53E-5	6.93E-5
a_1	1.05	1.40
a_2	1.17	1.55
n	0.293	0.223
Standard error	0.001715	0.001754
R^2	0.9429	0.9403

Table 21. Comparison of estimated parameters (gold leaching, Cu^{2+} as oxidant)

Model parameter	Estimated value	
	gPROMS	Modest
E, J/mol	7.97E+4	7.58E+4
k_{mean}, g/m^2 s	9.97E-4	1.68E-5
a_1	0.385	0.350
a_2	1.200	1.40
n	0.212	0.329
Standard error	0.0638	0.0328
R^2	0.9175	0.9474

The correlation matrix is used to evaluate the parameter estimation problem. The possible cross correlation between the estimated parameters can be observed from the correlation matrix produced using gPROMS as shown in Tables 22 and 23 respectively. Parameters with absolute value close to unity (1) indicate a high degree of correlation with each other and vice versa.

Table 22. Correlation matrix (gold leaching using RDE, Fe^{3+} as oxidant)

Parameter	No.	1	2	3	4	5
a_1	1	1				
a_2	2	-0.318	1			
E	3	-0.946	0.0189	1		
k_{mean}	4	-0.903	-0.005	0.980	1	
n	5	0.277	-0.00208	-0.192	0.00259	1

In this case, it can be seen that the model parameters a_1 and E and E and k_{mean} are in close correlation with each other.

Table 23. Correlation matrix (gold leaching using RDE, Cu^{2+} as oxidant)

Parameter	No.	1	2	3	4	5
a_1	1	1				
a_2	2	-0.996	1			
E	3	-0.451	0.499	1		
k_{mean}	4	-0.365	-0.408	-0.899	1	
n	5	0.345	-0.388	-0.907	0.999	1

In this case, it can be seen that the model parameters E_1 and E_2 and n and k_{mean} are in close correlation with each other.

Reactor modeling

The direct oxidation zinc concentrate (sphalerite) leaching process is simulated in Aspen Plus (v. 8.6) with the autoclave reactor being modeled as a series of continuous stirred tank reactors based on the Cominco reactor configuration. Such a configuration ensures that there is good dispersion of oxygen and the reaction mixture remains well agitated. The only disadvantage is the difficulty in maintaining constant temperature within the reactor. The sphalerite conversion at the end of the process is found to be 95.56 percent.

The sensitivity analysis was carried out for determining the optimum reactor operation temperature and the oxygen mass flow rate for obtaining maximum conversion as shown in figures 15 and 16 respectively.

From Figure 15, it can be observed that the optimum reactor operation temperature is 170 ^{0}C. This could be attributed to the fact that the oxidation of sphalerite concentrate is improved at higher temperatures thereby increasing the overall sphalerite conversion. Beyond 170 ^{0}C, no considerable improvement in the sphalerite conversion was observed.

From Figure 16, it can be clearly seen that the optimum oxygen mass flow for maximum conversion is found to be 21.6 kg/h. The oxygen consumption during the process seems to have an influence on the reaction rate and the conversion of sphalerite. High oxygen feed rates had a detrimental effect on the leaching conversion.

It has been presented in this study how to link the experimental data from zinc leaching eventually into the process simulation environment. The experimental data based reactor model is expected to strengthen the reliability of process design, optimization and troubleshooting tasks by simulations.

6 Conclusion

The main purpose of this thesis work was to evaluate the model building capabilities of gPROMS by carrying out mathematical process modeling of hydrometallurgical leaching processes like high pressure pyrite oxidation, direct oxidative zinc leaching and gold chloride leaching using rotating disc electrode (RDE). In each case, the parameter estimation was carried out and the reaction kinetic parameters were estimated.

Based on the model predictions obtained for each leaching case, it is observed that the predicted and experimental values are in good agreement with each other. The standard error and the coefficient of determination is found in each case to assess the model reliability. The coefficient of determination is found to be greater than 90 percent in each case showing relatively good fitting for the data. Also, the cross-correlation between the estimated parameters was checked by the use of a correlation matrix.

gPROMS was found to be an efficient simulation tool for process model development. In comparison to other commercial modeling software packages, gPROMS offered a more flexible and versatile modeling environment with its user friendly interface. The sophisticated numerical solvers incorporated within gPROMS were found to be quite reliable for carrying out detailed mathematical modeling and parameter estimation studies. The results obtained from the parameter estimations carried out in gPROMS correspond well with the values reported in literature. In addition to this, estimated parameter values using gPROMS have been compared with those obtained using the Modest program and both seem to be in close agreement.

The reactor modeling was done for the direct oxidation zinc concentrate leaching process. The autoclave reactor is based on the Cominco reactor configuration and has been modeled as continuous stirred tank reactors in series using Aspen Plus (v. 8.6). The sphalerite conversion was found to be 95.56 percent. In addition to this based on the sensitivity analysis carried out, the optimum reactor temperature was found to be 170 ^{0}C and the optimum oxygen mass flow rate is 21.6 kg/h. The reactor modeling demonstrated the implementation of experimental data based models into process flowsheet simulation environment.

References

Aspen Technology Inc (1981). Aspen Plus.
www.aspentech.com/products/engineering/aspen-plus

Aydogan, S., Aras, A. and Canbazoglu, M. (2005). Dissolution kinetics of sphalerite in acidic ferric chloride leaching. *Chemical Engineering Journal*, 114(1-3), pp.67-72.

Bailey, L. and Peters, E. (1976). Decomposition of pyrite in acids by pressure leaching and anodization: the case for an electrochemical mechanism. *Canadian Metallurgical Quarterly*, 15(4), pp.333-344.

Baldwin, S., Demopoulos, G. and Papangelakis, V. (1995). Mathematical modeling of the zinc pressure leach process. *MMTB*, 26(5), pp.1035-1047.

Björling, G., (1954). *Metall.*, Vol. 8, 781-784.

Chemstations Inc (1988). CHEMCAD.
www.chemstations.com

Derry, R. (1972). Pressure hydrometallurgy- A review. *Miner. Sci. Eng*. 4:3-24.

Dib, A. and Makhloufi, L. (2007). Mass transfer correlation of simultaneous removal by cementation of nickel and cobalt from sulfate industrial solution containing copper. *Chemical Engineering Journal*, 130(1), pp.39-44.

Feather, A., Sole, K.C. and Bryson, L.J. (1997). Gold refining by solvent extraction- the minataur process. *The Journal of the South African Institute of Mining and Metallurgy*, 97, pp.169-174.

Filippou, D. (2004). Innovative hydrometallurgical processes for the primary processing of zinc. *Mineral Processing and Extractive Metallurgy Review*, 25(3), pp.205-252.

Filmer, A.O., Lawrence, P.R. and Hoffmann, W. (1984). A Comparison of Cyanide, Thiourea and Chlorine as Lixiviant for Gold. Gold: Mining, Metallurgy and Geology, *The Australian Institute of Mining and Metallurgy*, p.279.

Forward, F. A. and Veltman, H., (1959). Direct leaching zinc-sulphide concentrates. *Journal of Metals*, pp.836-840.

Garrels, R. M.; Thompson, M. E. (1960). Oxidation of pyrite by iron sulfate solutions. *Aust. J. Sci*, 258-A, 57−67.

gPROMS (2005). gPROMS User Guide 2005: Process System Enterprise Ltd (PSE).

Haakana, T., Lahtinen, M., Takala, H., Ruonala, M. and Turunen, I. (2007). Development and modelling of a novel reactor for direct leaching of zinc sulphide concentrates. *Chemical Engineering Science*, 62(18-20), pp.5648-5654.

Haario, H. (2002). *Modest. User's Guide*; ProfMath Oy: Helsinki, Finland.

Holmes, P. and Crundwell, F. (2000). The kinetics of the oxidation of pyrite by ferric ions and dissolved oxygen: an electrochemical study. *Geochimica et Cosmochimica Acta*, 64(2), pp.263-274.

Kammel, R., Pawlek, F., Simon,M., Xi-Ming, L. (1987). Oxidizing leaching of sphalerite under atmospheric pressure. *Metall 41*, p.158-161

Kaskiala, T. (2005). Determination of mass transfer between gas and liquid in atmospheric leaching of sulphidic zinc concentrates. *Minerals Engineering*, 18(12), pp.1200-1207.

Kazanbaev, L., Kozlov, P., Kubasov, V. (2007). Hydrometallurgy of zinc, Leaching processes (in Russian). *Moscow: Ore and Metals*, p. 120.

Levenspiel, O. (1999). *Chemical reaction engineering*. New York: Wiley.

Long, H. and Dixon, D. (2004). Pressure oxidation of pyrite in sulfuric acid media: a kinetic study. *Hydrometallurgy*, 73(3-4), pp.335-349.

Mackiw, V.N., and Veltman, H., Can.Mining Met.Bull. 60(1967), p. 80-85. Ref. Jan, R., Hepworth, M. T., Fox, V. G. (1976). A Kinetic Study on the Pressure Leaching of Sphalerite. Metallurgical Transactions, p. 353 – 361.

Maslenetsky, I., Dolivo-Dobrovolsky, V., Dobrohotov, G., Sobol, S., Chugaev, L., Belikov, V. (1969). Autoclave processes in nonferrous metallurgy (in Russian), *Moscow: Metallurgy*, p. 399

MathWorks Inc (1984). MATLAB.
www.mathworks.com/products/matlab

Moses, C., Kirk Nordstrom, D., Herman, J. and Mills, A. (1987). Aqueous pyrite oxidation by dissolved oxygen and by ferric iron. *Geochimica et Cosmochimica Acta*, 51(6), pp.1561-1571.

Process Systems Enterprise (1997). gPROMS.
www.psenterprise.com/gproms.

Singer, P.C. and Stumm, W. (1970). The solubility of ferrous iron in carbonate bearing waters. *J. Am. Water. Works Ass*. 62, 198–202.

Sequeira, C. and Marquis, F. (1997). Chemistry, energy and the environment. Proceedings of the Third European Workshop on Chemistry, Energy and Environment, *Estoril: Royal Society of Chemistry*, p. 531.

Souza, A., Pina, P., Leão, V., Silva, C. and Siqueira, P. (2007). The leaching kinetics of a zinc sulphide concentrate in acid ferric sulphate. *Hydrometallurgy*, 89(1-2), pp.72-81.

Sulaymon, A. and Abbar, A. (2012). *Journal of Electrochemical Science and Technology*, 3(4), pp.165-171.

Takala, H. (1999), Leaching of Zinc Concentrates at Outokumpu Kokkola Plant. ERZMETALL, p. 52

Tijl, P. (2005). *Capabilities of gPROMS and Aspen Custom Modeler, Using the SecButyl-Alcohol Stripper Kinetics Case Study*. Graduation report, Eindhoven Technical University.

Tromans, D. (1998). Oxygen solubility modeling in inorganic solutions: concentration, temperature and pressure effects. *Hydrometallurgy*, 50(3), pp.279-296.

Van Weert, G. (1989). Chloride and nitrate systems in hydrometallurgy – applications and opportunities. Doctoral Thesis, Technical University of Delft, The Netherlands (236p).

Veltman, H.,Gulyas, J.W., O'Kane, P.T., Middagh, W.R. (1972). *Can*. 904, p. 591. Ref. Jan, R., Hepworth, M. T., Fox, V. G. (1976). A Kinetic Study on the Pressure Leaching of Sphalerite. *Metallurgical Transactions*, p. 353 - 361

Verbaan, B. and Crundwell, F. (1986). An electrochemical model for the leaching of a sphalerite concentrate. *Hydrometallurgy*, 16(3), pp.345-359.

Xie, K., Yang, X., Wang, J., Yan, J. and Shen, Q. (2007). Kinetic study on pressure leaching of high iron sphalerite concentrate. *Transactions of Nonferrous Metals Society of China*, 17(1), pp.187-194.

Yuan-Hui, L. and Gregory, S. (1974). Diffusion of ions in sea water and in deep-sea sediments. *Geochimica et Cosmochimica Acta*, 38(5), pp.703-714.

Zhukov, V.V., Laari, A. and Koiranen, T. (2015). Kinetic Modeling of High-Pressure Pyrite Oxidation with Parameter Estimation and Reliability Analysis Using the Markov Chain Monte Carlo Method. *Industrial & Engineering Chemistry Research*, 54(41), pp.9920-9930.

APPENDICES

Appendix I: High pressure pyrite oxidation gPROMS template

Appendix II: Zinc concentrate leaching gPROMS template

Appendix III: Gold leaching using rotating disc electrode (RDE) gPROMS template

Appendix IV: Stream compositions at reactor outlet

Model template

PARAMETER

 # Parameter Definition

Density AS REAL
Tm AS REAL
C1m AS REAL
C2m AS REAL
C3m AS REAL
Xm AS REAL
Dm AS REAL
MFes2 AS REAL
RhoH2O AS REAL
RhoH2SO4 AS REAL
CH2SO4 AS REAL
Vs AS REAL
R AS REAL
N2 AS REAL
N3 AS REAL
N4 AS REAL
N5 AS REAL

VARIABLE

#Variable Definition

A AS Area
P AS Pressure
X AS Conv
Ci AS FirstPyriteConc
C1 AS O2Conc
C2 AS FerrousConc
C3 AS FerricConc
Psi AS NoType
A1 AS NoType

Patm AS NoType
VFes2 AS VolPyrite
Vws AS VolWaterFrac
EH2SO4 AS VolFracAcid
VH2SO4 AS VolAcid
EH2O AS VolSol
WCH2SO4 AS MolalityAcid
Es AS VolFracSol
N AS ParticleNumber
R1 AS NoType
R2 AS NoType
R3 AS NoType
R33 AS NoType
K1 AS NoType
K2 AS NoType
K3 AS NoType
Keq AS NoType
T AS Temp
MSFes2 AS PyriteConc
Dp AS ParticleDia
F3F2 AS FerrousFerricRatio
F3Ft AS FeRatio

Parameter Estimation

Fpre AS NonFr
K1m AS NoType
K2m AS NoType
K3m AS NoType
N1 AS NoType
E1 AS NoType
E2 AS NoType
E3 AS NoType

SET

EQUATION

Initial pyrite concentration, Ci

Ci = MSFes2/MFes2 ;

Surface reaction rate between pyrite and oxygen, R1

R1 = (K1*N*A)*(((1-X)/Xm)^N1) * ((C1/C1m))^N2 ;

Surface reaction rate between pyrite and ferric ions, R2

R2 = (N*A*K2)*(((1-X)/Xm)^N1) * ((C3/C3m))^N3 ;

Reaction rate for reaction between ferrous iron and oxygen, R3

R3 = K3*((C2/C2m)^N4) * ((C1/C1m))^N5 ;

Backward reaction (ferric iron to ferrous iron) rate, R33

R33 = (K3/Keq) * ((C3/C2m)^N4) ;

Rate constant 1, K1

K1 = K1m *EXP((-E1*((1/T)-(1/Tm))/R)) ;

Rate Constant 2, K2

K2 = K2m *EXP((-E2*((1/T)-(1/Tm))/R)) ;

Rate Constant 3, K3

K3 = K3m *EXP((-E3*((1/T)-(1/Tm))/R)) ;

Differential Mass Balance, dX/dt

$X = (R1 + R2)/Ci ;

Ferrous iron production rate, dFe2+/dt

$C2 = (15*R2/Es) - R3 + R33 ;

Ferric iron production rate, dFe3=/dt

$C3 = -(14*R2/Es) + ((Fpre * R1)/Es) + R3 - R33 ;

Constant 1, Psi

Psi = (1/(1 + 2.01628*WCH2SO4))^0.168954 ;

Constant 2, A1

A1 = EXP((((0.046*T^2) + (203.357*T*LOG(T/298) - (299.378 + (0.092*T)) * (T-298) - 20591))/(8.3143*T)) ;

Constant 3, Patm

Patm = P/101.325 ;

O2 Concentration, C1

C1 = Psi*Patm*A1 ;

Volume of pyrite, VFes2

VFes2 = (MSFes2 * Vs)/Density ;

Volume fraction of water, Vws

Vws = Vs - VFes2 ;

Volume fraction of acid, EH2SO4

EH2SO4 = CH2SO4/RhoH2SO4 ;

Volume of acid, VH2SO4

VH2SO4 = EH2SO4*Vws ;

 # Volume of solution, EH2O

EH2O = (Vws - VH2SO4)/Vws ;

 # Molality of Acid, WCH2SO4

WCH2SO4 = CH2SO4*EH2O/RhoH2O ;

 # Volume fraction of solution, Es

Es = Vws/Vs ;

 # Particle Number, N

N = (VFes2*0.001)/((3.1415/6)*Dp^3);

 # Area, A

A = (3.1415*(1-X)^(2/3))* (Dp^2);

 # Ferric to Ferrous ratio, F3F2

F3F2 = F3Ft/(1 - F3Ft) ;

 # Equlibrium Constant, Keq

Keq = (F3F2^N4)*((C1/C1m)^(- N5)) ;

Process Template

UNIT

C101 AS presox

SET

WITHIN C101 DO

Density := 4800 ;
Tm := 483.15 ;
C1m := 0.01 ;
C2m := 1E-3 ;
C3m := 2.5E-3 ;
Xm := 0.5 ;
Dm := 62.6E-6 ;
R := 8.314 ;
Vs := 1 ;
MFes2 := 119.98 ;
CH2SO4 := 0.5 ;
RhoH2SO4 := 1840 ;
RhoH2O := 850 ;
N2:= 0.5 ;
N3 := 1 ;
N4 := 2 ;
N5 := 0.5 ;

END

ASSIGN

WITHIN C101 DO

K1m := 0.279E-1 ;
K2m := 0.269E-2 ;
K3m := 0.841E-4 ;

```
E1 := 0.469E+5 ;
E2 := 0.414E+5 ;
E3 := 0.134E+6 ;
N1 := 0.503 ;
Dp := 62.6E-6;
T := 443.15;
P := 690 ;
MSFes2 := 1;
F3Ft := 0.801;
Fpre := 0.10 ;
END

INITIAL

WITHIN C101 DO
X = 0.14;
C2 = 1E-9 ;
C3 = 1E-6;

END
```

Parameter Estimation Template

Experiments to be included in estimation

EXPERIMENTS

No1
No2
No3
No4
No5
No6
No7
No8
No9
No10

Parameters to be estimated

ESTIMATE

C101.E1
46900.0 : 10000.0 : 100000.0

ESTIMATE

C101.E2
41400.0 : 10000.0 : 500000.0

ESTIMATE

C101.E3
134000.0 : 10000.0 : 250000.0

ESTIMATE

C101.Fpre

0.3 : 0.3 : 0.7
ESTIMATE

C101.K1m
0.0279 : 0.02 : 1.0

ESTIMATE

C101.K2m
0.00269 : 1.0E-4 : 0.0050

ESTIMATE

C101.K3m
8.41E-5 : 1.0E-6 : 2.0E-4

ESTIMATE

C101.N1
0.503 : 0.0 : 1.0

Model Template

PARAMETER

Parameter definition

R AS REAL
ms AS REAL
mfZn AS REAL
mfFe AS REAL
roos AS REAL
MZn AS REAL
MFe AS REAL
MO2 AS REAL
MH2SO4 AS REAL
kO2 AS REAL
Tm AS REAL
vism AS REAL
csam AS REAL
k3 AS REAL
e3 AS REAL
cZnini AS REAL
sto1 AS REAL
sto2 AS REAL

VARIABLE

Variable definition

fZn AS NoType
T AS Temp
k1m AS NoType
k2m AS NoType
e1 AS NoType
e2 AS NoType
n4 AS Constant
n1 AS Constant
n2 AS Constant

n3 AS Constant
Z AS NoType
k1 AS NoType
k2 AS NoType
r1 AS NoType
r2 AS NoType
r3 AS NoType
cr1 AS NoType
cr2 AS NoType
cr3 AS NoType
vis AS NoType
n AS NoOfPar
cZn AS ZnConc
V AS NoType
r31 AS NoType
cFe2 AS Fe2Conc
cFe3 AS Fe3Conc
cH AS HConc
X AS Conv
ai AS Area
ri AS parrad
Dp AS inipardia
di AS ParDia
csa AS H2SO4Conc
csa1 AS H2SO4Conc1
pO2 AS O2PR
cO2 AS O2Conc
par1 AS NoType
m AS NoType
r0 AS NoType
ar AS NoType
aii AS NoType
dii AS NoType
De AS NoType
De1 AS NoType
rs1 AS NoType
rs2 AS NoType
rm1 AS NoType

rm2 AS NoType
cO2s AS NoType
cFe3s AS NoType
rpar AS NoType

SET

EQUATION

Dissolved oxygen concentration, cO2

cO2 = pO2 * kO2 ;

Concentration of H2SO4, csa1

csa1 = (csa/MH2SO4) ;

Constant 1

par1 = (Dp ^3) * (cZn/cZnini) ;

Inner diameter of particle, di

di = (par1) ^ (1/3) ;

Inner radius of particle, ri

ri = (di/2) ;

#
ai = 3.1415 * (di ^2) ;

Constant 2, Z

Z = (1/R) *((1/T) - (1/Tm));

Rate constant 1, k1

k1 = k1m * EXP(-e1*Z) ;

Rate constant 2, k2

k2 = k2m * EXP(-e2*Z) ;

Mass fraction of zinc

fZn = mfZn/100 ;

Reaction rate at the surface for zinc oxidation by oxygen, r1

r1 = k1 * fZn * (cO2s ^n1) * (cH ^n2) ;

Reaction rate at the surface for zinc oxidation by ferric iron, r2

r2 = k2 * fZn * (cFe3s ^n3) * (cH ^n4) ;

cr1 = cFe2 / 1000 ;

cr2 = cO2 / 1000 ;

cr3 = cH / 1000 ;

Reaction rate at the surface for zinc oxidation by ferrous iron, r3

r3 = k3 * EXP(-e3/(R*T))*(cr1^2)* cr2 * (cr3^(-0.35)) ;

r31 = r3*1000 ;

Zn production rate, dcZn/dt

$cZn = -(r1 + r2) * ai * n ;

Ferric iron production rate, dcFe3/dt

$cFe3 = -(2*r2*ai*n) + r31 ;

Ferrous iron production rate, dcFe2/dt

$cFe2 = (mfFe/mfZn) * (MZn / MFe) * (r1+r2)*ai*n + 2*r2*ai*n - r31 ;

H2SO4 production rate, dcH/dt

$cH = -(2*r1) - (2*r31) ;

Conversion, X

X = 100 *((cZnini - cZn) / cZnini) ;

Diffusion coefficient, De1

De1 = De * (1E-9) * (vism / vis) * (T/Tm) ;

Volume, V

V = (3.1415 * (Dp ^3) / 6);

Mass, m

m = V *roos ;

Number particles per unit volume, n

n = ms/m ;

Outer particle radius, r0

r0 = Dp / 2 ;

ar = 3.1415 * (Dp ^ 2) ;

Outer surface gradient

rpar = ri / ((r0 - ri)*r0) ;

dii = 2 *ri ;

aii = 3.1415 * (dii ^ 2) ;

Surface reaction rate, rs1

rs1 = sto1 * k1 * fZn * (cO2s ^n1) * (csa ^ n2)*aii ;

Mass transfer rate (O2 as oxidant), rm1

rm1 = De*rpar*(cO2 - cO2s)*ar ;

Oxygen balance at reacting surface, dcO2s/dt

$cO2s = rs1 - rm1 ;

Surface reaction rate (Fe3+ as oxidant), rs2

rs2 = sto2 * k2 * fZn * (cFe3s ^n3) * (csa ^ n4)*aii ;

Mass transfer rate (Fe3+ as oxidant), rm2

rm2 = De*rpar*(cFe3 - cFe3s)*ar ;

Fe3 balance at reacting surface

$cFe3s = rs2 - rm2 ;

Process Template

UNIT

R101 AS znModel

SET

WITHIN R101 DO

R := 8.314 ;
ms := 5 ;
mfZn := 0.4085 ;
mfFe := 0.1521 ;
roos := 4000 ;
Mzn := 65.409E-3 ;
MFe := 55.845E-3 ;
MO2 := 32E-3 ;
MH2SO4 := 98.078E-3 ;
kO2 := 4 ;
k3 := 124.89E+9 ;
e3 := 6.8E+4 ;
Tm := 403 ;
vism := 2.12 ;
csam := 75 ;
cZnini := 0.31226 ;
sto1 := 0.5 ;
sto2 := 2 ;

END

ASSIGN

WITHIN R101 DO

k1m := 0.45E-2 ;
k2m := 0.1E-6;
e1 := 0.58E+5 ;

```
e2 := 0.45E+6 ;
n1 := 0.56 ;
n2 := -0.4 ;
n3 := 0.57 ;
n4 := 0.8 ;
Dp := 40E-6 ;
T := 413 ;
pO2 := 1.4 ;
csa := 50 ;
vis := 1.955 ;
De := 2.63E-1 ;

END

INITIAL

WITHIN R101 DO

$cO2s = 0 ;
$cFe3s = 0 ;
cZn = 0.31226 ;
cFe2 = 0 ;
cFe3 = 0 ;
cH = 1019.57 ;

END
```

Parameter estimation template

 # Experiments to be included

EXPERIMENTS

E1
E2
E3
E4
E5
E6
E7
E8
E9
E10
E11
E12
E13
E14
E15
E16
E17
E18
E19
E20
E21
E22

 # Parameters to be estimated

ESTIMATE

R101.De
9.0E-10 : 1.0E-20 : 3.0E-9

ESTIMATE

R101.e1
65300.0 : 30000.0 : 80000.0

ESTIMATE

R101.e2
98500.0 : 1.0 : 200000.0

ESTIMATE

R101.k1m
0.0076 : 1.0E-6 : 0.03

ESTIMATE

R101.k2m
5.41E-9 : 1.0E-12 : 2.0E-6

ESTIMATE

R101.n4
0.8 : 0.4 : 1.8

Case 1: Gold leaching using Fe^{3+}

Model Template

PARAMETER

Parameter definition

Tm AS REAL
Rem AS REAL
dc AS REAL
Rho AS REAL
Tref AS REAL
Dref AS REAL
myyref AS REAL
Mau AS REAL
R AS REAL

VARIABLE

Variable definition

C1 AS BulkConc
km AS NoType
E AS NoType
n1 AS NoType
a1 AS NoType
a2 AS NoType
rpm AS RPM
Temp AS Temperature
myy AS DV
nyy AS KV
nr AS RPS
Df AS NoType
rr AS Rate
rr1 AS Rate
Re AS NoType
Sc AS NoType

Sh AS NoType
KL AS MassTransferCoeff
Cs AS ConcSurface
k AS RateConstant
rs AS NoType
rm AS NoType

SET

EQUATION

Speed of rotation of electrode, rps

nr = rpm/60 ;

Kinematic viscosity, nyy

nyy = myy/Rho ;

Diffusion coefficient, Df

Df = Dref * (myyref/myy) * (Temp/Tref) ;

Leaching rate, rr1

rr1 = rr/Mau ;

Reynolds number, Re

Re = (3.1415 * nr * (dc^2))/nyy ;

Schmidt number, Sc

Sc = nyy/Df ;

Sherwood number, Sh

Sh = a1 * ((Re/Rem)^a2) * (Sc^(1/3)) ;

 # Mass transfer coefficient across boundary layer, KL

KL = (Sh * Df)/dc ;

 # Surface concentration differential, dCs/dt

$Cs = rs - rm ;

 # Surface reaction rate, rs

rs = (k * Cs ^n1) ;

 # Mass transfer rate, rm

rm = KL * (C1 - Cs) ;

 # Rate constant, k

k = km * EXP((E/R) * ((1/Temp) - (1/Tm))) ;

 # Surface concentration, Cs

Cs = (KL * C1 - rr1)/KL ;

Process template

UNIT

R101 AS GoldLeach

SET

WITHIN R101 DO
Mau := 197 ;
Tm := 353.15 ;
Rem := 350 ;
dc := 4.08E-3 ;
Rho := 972 ;
Tref := 298.15 ;
Dref := 6.07E-9 ;
myyref := 0.890E-3 ;
R := 8.314 ;
END

ASSIGN

WITHIN R101 DO
rpm := 100 ;
myy := 3.78E-4 ;
Temp := 348.15 ;
km := 0.697E-4 ;
E := 0.391E+5 ;
n1 := 0.227 ;
a1 := 1.41 ;
a2 := 1.55 ;
C1 := 0.50 ;
END

INITIAL
STEADY_STATE

Parameter Estimation Template

 # Experiments to be included

EXPERIMENTS

N1
N2
N3
N4
N5
N6
N7

 # Parameters to be estimated

ESTIMATE

R101.a1
1.41 : 0.0010 : 100.0

ESTIMATE

R101.a2
1.55 : 0.4 : 3.0

ESTIMATE

R101.E
39100.0 : 1000.0 : 100000.0

ESTIMATE

R101.km
6.97E-5 : 1.0E-12 : 6.0E-4

ESTIMATE

R101.n1
0.227 : 0.01 : 0.7

Case 2: Gold leaching using Cu^{2+}

Model Template

PARAMETER

Parameter definition

Tm AS REAL
Rem AS REAL
dc AS REAL
Rho AS REAL
Tref AS REAL
Dref AS REAL
myyref AS REAL
Mau AS REAL
R AS REAL

VARIABLE

Variable definition

C1 AS BulkConc
km AS NoType
E AS NoType
n1 AS NoType
a1 AS NoType
a2 AS NoType
rpm AS RPM
Temp AS Temperature
myy AS DV
nyy AS KV
nr AS RPS
Df AS NoType
rr AS Rate
rr1 AS Rate
Re AS NoType
Sc AS NoType

Sh AS NoType
KL AS MassTransferCoeff
Cs AS ConcSurface
k AS RateConstant
rs AS NoType
rm AS NoType

SET

EQUATION

Speed of rotation of electrode, rps

nr = rpm/60 ;

Kinematic viscosity, nyy

nyy = myy/Rho ;

Diffusion coefficient, Df

Df = Dref * (myyref/myy) * (Temp/Tref) ;

Leaching rate, rr1

rr1 = rr/Mau ;

Reynolds number, Re

Re = (3.1415 * nr * (dc^2))/nyy ;

Schmidt number, Sc

Sc = nyy/Df ;

Sherwood number, Sh

Sh = a1 * ((Re/Rem)^a2) * (Sc^(1/3)) ;

 # Mass transfer coefficient across boundary layer, KL

KL = (Sh * Df)/dc ;

 # Surface concentration differential, dCs/dt

$Cs = rs - rm ;

 # Surface reaction rate, rs

rs = (k * Cs ^n1) ;

 # Mass transfer rate, rm

rm = 3*KL * (C1 - Cs) ;

 # Rate constant, k

k = km * EXP((E/R) * ((1/Temp) - (1/Tm))) ;

 # Surface concentration, Cs

Cs = (KL * C1 - rr1)/KL ;

Process Template

UNIT

R101 AS AuLeach

SET

WITHIN R101 DO
Tm := 353.15 ;
Rem := 350 ;
dc := 4.08E-3 ;
Rho := 972 ;
Tref := 363.15 ;
Dref := 7.33E-9 ;
myyref := 0.315E-3 ;
R := 8.314 ;
END

ASSIGN

WITHIN R101 DO
rpm := 100 ;
myy := 3.78E-4 ;
Temp := 348.15 ;
km := 0.27E-4 ;
E := 0.789E+5 ;
n1 := 0.391 ;
a1 := 0.437 ;
a2 := 1.28 ;
C1 := 0.50 ;
END

INITIAL

STEADY_STATE

Parameter estimation template

 # Experiments to be included

EXPERIMENTS

n1
n2
n3
n4
n5
n6
n7
n8

 # Parameters to be estimated

ESTIMATE

R101.a1
0.437 : 0.1 : 0.8

ESTIMATE

R101.a2
1.28 : 0.8 : 1.8

ESTIMATE

R101.E
78900.0 : 1000.0 : 1000000.0

ESTIMATE

R101.km
2.7E-5 : 2.0E-15 : 0.001

ESTIMATE

R101.n1
0.391 : 0.01 : 0.8

Property Method: UNIQUAC

Acid Concentration: 50 mg/L

Table 24. Stream composition at reactor outlet

Stream composition at outlet (kg/h)				
Component	Reactor 1	Reactor 2	Reactor 3	Reactor 4
$ZnSO_4$	9.084562	15.87107	22.75232	28.48772
H_2O	1.013672	1.770922	2.538744	3.17871
S	1.804268	3.152124	4.518796	5.657893
O_2	20.69976	41.62724	62.54534	61.97698
ZnS	12.51641	8.419964	4.266334	0.8043533
Temperature (^{0}C)	170	170	170	170
Pressure (Bar)	12.5	12.5	12.5	12.5